nature aging

Article

https://doi.org/10.1038/s43587-025-00811-7

A BCL-xL/BCL-2 PROTAC effectively clears senescent cells in the liver and reduces MASH-driven hepatocellular carcinoma in mice

Received: 2 March 2023

Accepted: 5 December 2024

Published online: 31 January 2025

Check for updates

Yang Yang[1,2,9], Natacha Jn-Simon[3,9], Yonghan He[4,9], Chunbao Sun[3], Peiyi Zhang[5], Wanyi Hu[5], Tian Tian[3], Huadong Zeng[6], Sreenivasulu Basha[3], Araceli S. Huerta[7], Lu-Zhe Sun[7], Xian-Ming Yin[3], Robert Hromas[8], Guangrong Zheng[5], Liya Pi[3] ✉ & Daohong Zhou[1,4] ✉

Accumulation of senescent cells (SnCs) plays a causative role in many age-related diseases and has also been implicated in the pathogenesis and progression of metabolic dysfunction-associated steatotic liver disease (MASLD). Senolytics that can selectively kill SnCs have the potential to be developed as therapeutics for these diseases. Here we report the finding that 753b, a dual BCL-xL/BCL-2 proteolysis-targeting chimera (PROTAC), acts as a potent and liver-tropic senolytic. We found that treatment with 753b selectively reduced SnCs in the liver in aged mice and STAM mice in part due to its sequestration in the liver. Moreover, 753b treatment could effectively reduce the progression of MASLD and the development of hepatocellular carcinoma (HCC) in STAM mice even after the mice developed substantial metabolic dysfunction-associated steatohepatitis (MASH) and hepatic fibrosis. These findings suggest that BCL-xL/BCL-2 PROTACs have the potential to be developed as therapeutics for MASLD to reduce MASH-driven HCC.

Senescent cells (SnCs) have emerged as potential therapeutic targets of aging and various human diseases[1,2]. This is because accumulation of SnCs causes chronic oxidative stress and inflammation via increased production of reactive oxygen species and expression of the senescence-associated secretory phenotype (SASP), which drives pathology[1,2]. Agents that can selectively kill SnCs, termed senolytics, have the potential to be developed as therapeutics for some of these diseases.

Metabolic dysfunction-associated steatotic liver disease (MASLD) is a fast-growing chronic liver disease, affecting 25–30% of the population in Western countries[3]. MASLD has a broad spectrum of liver pathologies, ranging from non-alcoholic fatty liver or steatosis to metabolic dysfunction-associated steatohepatitis (MASH), fibrosis/cirrhosis and hepatocellular carcinoma (HCC)[3,4]. Advanced forms of MASLD, such as cirrhosis and HCC, often require liver transplantation and are one of the major causes of liver-related deaths[5]. Therapeutics

[1]Department of Biochemistry and Structural Biology, University of Texas Health Science Center, San Antonio, TX, USA. [2]Department of Pharmacology and Therapeutics, College of Medicine, University of Florida, Gainesville, FL, USA. [3]Department of Pathology, Tulane University, New Orleans, LA, USA. [4]Department of Pharmacodynamics, College of Pharmacy, University of Florida, Gainesville, FL, USA. [5]Department of Medicinal Chemistry, College of Pharmacy, University of Florida, Gainesville, FL, USA. [6]Advanced Magnetic Resonance Imaging and Spectroscopy Facility, University of Florida, Gainesville, FL, USA. [7]Department of Cell Systems and Anatomy, University of Texas Health Science Center, San Antonio, TX, USA. [8]Department of Medicine, University of Texas Health Science Center, San Antonio, TX, USA. [9]These authors contributed equally: Yang Yang, Natacha Jn-Simon, Yonghan He. ✉e-mail: lpi@tulane.edu; zhoud@uthscsa.edu

that can prevent the progression of MASLD from MASH to cirrhosis and HCC have the potential to reverse the course of the disease and are in urgent need. Unfortunately, most of the phase 3 clinical trials testing new therapeutics for MASH have failed[6], except resmetirom, which was able to improve liver fibrosis and prevent the worsening of the MASLD score[7]. As such, resmetirom is the only drug approved by the FDA for MASH. Recently, an increasing body of evidence suggests that SnC accumulation may play a critical role in the induction and progression of MASLD[8–10]. Therefore, senolytics that can effectively clear SnCs in the liver can be exploited as therapeutics to treat MASH and to reduce MASH-driven HCC.

Since 2015, several senolytic agents have been identified[11–13], including natural compounds and their derivatives, small-molecule inhibitors and β-galactosidase-targeted prodrugs. Among these small-molecule senolytics, ABT263 is perhaps the most potent and broad-spectrum senolytic[14]. It can potently kill a variety of SnCs with a few exceptions, such as senescent chondrocytes[15], synovial fibroblasts[15] and preadipocytes (PACs)[16]. It can also effectively clear SnCs in various murine tissues. Clearance of SnCs with ABT263 can rejuvenate the function of various tissue stem cells in aged mice[14] and ameliorate several pathological conditions associated with aging, such as atherosclerosis, dementia and pulmonary fibrosis in mouse models[17–19]. Similar findings were also observed in mice after treatment with ABT737, a predecessor and preclinical drug candidate of ABT263 (refs. 20–23). However, the on-target toxicity of thrombocytopenia induced by BCL-xL inhibition prevents the use of ABT263 and other BCL-xL-specific inhibitors in the clinic, even for patients with cancer, because platelets also depend on BCL-xL for survival[24–27]. To reduce its on-target platelet toxicity, we previously converted ABT263 into PZ15227, a proteolysis-targeting chimera (PROTAC) that targets BCL-xL to the E3 ligase cereblon for ubiquitination and degradation. PZ15227 exhibits a significantly reduced platelet toxicity because platelets express lower levels of cereblon than other cells[11]. However, PZ15227 shows a moderate improvement in its senolytic activity compared to ABT263, probably because it degrades only BCL-xL, and many SnCs co-depend on BCL-xL, BCL-2 and BCL-w for survival[14,16,20].

Recently, we generated a dual BCL-xL and BCL-2 degrader, 753b, which can potently degrade BCL-xL and BCL-2 via the VHL E3 ligase[28]. We evaluated the senolytic activity of 753b in vitro and in vivo not only in naturally aged mice but also in STAM mice, a mouse model for MASLD induced by a single injection of streptozotocin (STZ) on postnatal day 2 (P2) followed by high-fat diet (HFD) feeding starting on P30 (refs. 29,30). The results from these studies are reported below.

Results

753b is a potent senolytic agent

Because many SnCs are co-dependent on BCL-xL and BCL-2 for survival[14], we evaluated whether 753b can be used as a senolytic agent that can more potently kill SnCs by degrading BCL-xL and BCL-2 than ABT263. Initially, we evaluated the half-maximal degradation concentration (DC_{50}) and maximum level of target degradation (D_{max}) of 753b for various BCL-2 family anti-apoptotic proteins, including BCL-xL, BCL-2, BCL-w and MCL-1 in non-senescent WI-38 fibroblast cells (NC WI-38 cells) to confirm that 753b is a potent dual BCL-xL and BCL-2 PROTAC (Extended Data Fig. 1a,b). Our results from this assay show that 753b can potently degrade BCL-xL and, at higher concentrations, BCL-2 and BCL-w, whereas it has no significant effect on the levels of MCL-1. Next, we compared the effects of 753b on the levels of BCL-xL, BCL-2 and BCL-w in ionizing radiation-induced senescent WI-38 cells (IR-SnC WI-38 cells) and NC WI-38 cells. Compared to NC WI-38 cells, IR-SnC WI-38 cells exhibited a slight upregulation of BCL-xL but a downregulation of BCL-2 and MCL-1 (Extended Data Fig. 1c), which may partially contribute to the higher sensitivity of SnCs to BCL-xL inhibition or degradation than non-SnCs. Treatment of these cells with 753b up to 100 nM induced a dose-dependent degradation of BCL-xL in both cell types, with a DC_{50} value of 2.81 nM for IR-SnC WI-38 cells and 4.81 nM for NC WI-38 cells (Fig. 1a–c). 753b also reduced the levels of BCL-2 in IR-SnC WI-38 cells but not in NC WI-38 cells, whereas it had no significant effect on BCL-w in either cell type, even at 100 nM concentration. Similar results were also observed in these cells when they were incubated with 50 nM 753b for various durations (Fig. 1d,e), suggesting that 753b is slightly more effective at degrading BCL-xL and BCL-2 in IR-SnC WI-38 cells than in NC WI-38 cells. This difference is not attributable to the differential expression of the E3 ligase recruited by 753b to degrade these proteins because both cell types express similar levels of VHL (Extended Data Fig. 1c). On the other hand, human platelets show minimal expression of VHL and are less sensitive to 753b-induced BCL-xL degradation and toxicity, as we previously reported[28]. In addition, we confirmed that both BCL-xL and BCL-2 degradation induced by 753b in NC WI-38 cells and IR-SnC WI-38 cells depends on binding to BCL-xL/BCL-2 and VHL because pre-incubation of the cells with ABT263 and VHL ligand (VHL-L) to compete with 753b for BCL-xL/BCL-2 and VHL binding, respectively, can block BCL-xL and BCL-2 degradation (Fig. 1f). Furthermore, inhibition of proteasome activity with MG132 also blocked their degradation, confirming that 753b induces degradation of BCL-xL/BCL-2 through the ubiquitin–proteasome system. Together, these results indicate that 753b-induced degradation requires binding to BCL-xL/BCL-2 and VHL and a functional ubiquitin–proteasome system.

Next, we evaluated the potency of 753b and ABT263 against NC, IR-SnC and replicative senescent (REP-SnC) WI-38 cells (Fig. 1g). As we reported previously, ABT263 is more toxic to both IR-SnC and REP-SnC WI-38 cells than NC WI-38 cells[14]. Compared to ABT263, 753b is less cytotoxic to NC WI-38 cells but more potent than ABT263 against IR-SnC and REP-SnC WI-38 cells. Indeed, multiple repeat assays showed that 753b is about 14-fold more potent than ABT263 against IR-SnC WI-38 cells (Fig. 1g), which is likely attributable to the induction of apoptosis as evidenced by the induction of Caspase 3 cleavage (Fig. 1h). Similar results were also observed in human renal epithelial cells (RECs) and human umbilical vein endothelial cells (HUVECs), confirming that 753b is a more potent senolytic agent than ABT263 and has a broad senolytic activity against SnCs derived from different tissue origins and induced by different triggers (Extended Data Fig. 1d,e). However, 753b and ABT263 are not senolytic to senescent PACs induced by irradiation (IR) (Extended Data Fig. 1f) because senescent PACs are not dependent on BCL-xL and BCL-2 for survival, as reported previously[16,31]. In contrast, senescent PACs are sensitive to dasatinib (D) and quercetin (Q) (Extended Data Fig. 1g)[16,31]. These findings demonstrate that, by converting ABT263 into a VHL-based PROTAC, we can improve its senolytic activities as well as its anti-tumor activity reported in our previous studies[11,28] while reducing its toxicity not only to platelets but also to various normal cells[14,32].

753b reduces senescence burden in a tissue-specific manner

After confirming that 753b is a potent and broad-spectrum senolytic in vitro, we investigated whether 753b can effectively clear SnCs in vivo in naturally aged mice, as depicted in Fig. 2a. We adopted a less intensive dosing regimen (5 mg kg^{-1}, once every 3 d (q3d), intraperitoneally (IP)) for 753b treatment in this study considering that 753b is more potent and has a longer-lasting effect as a PROTAC than ABT263, which requires daily oral administration at 50 mg kg^{-1} or higher to be therapeutically effective. First, we evaluated the toxicity of 753b to platelets by measuring platelet counts in blood collected from aged mice 1 d after the first and last injections of vehicle or 753b in comparison to platelet counts in blood from untreated young mice. The results showed that vehicle-treated aged mice had significantly higher levels of platelets in blood than young mice (Fig. 2b). Treatment of 753b reduced blood platelets in aged mice to a level similar to that in untreated young mice. However, the reduction of blood platelet counts after 753b treatment was less severe than that seen after ABT263 treatment, as we previously reported[28], confirming that 753b is less toxic to platelets than ABT263.

https://doi.org/10.1038/s43587-025-00811-7

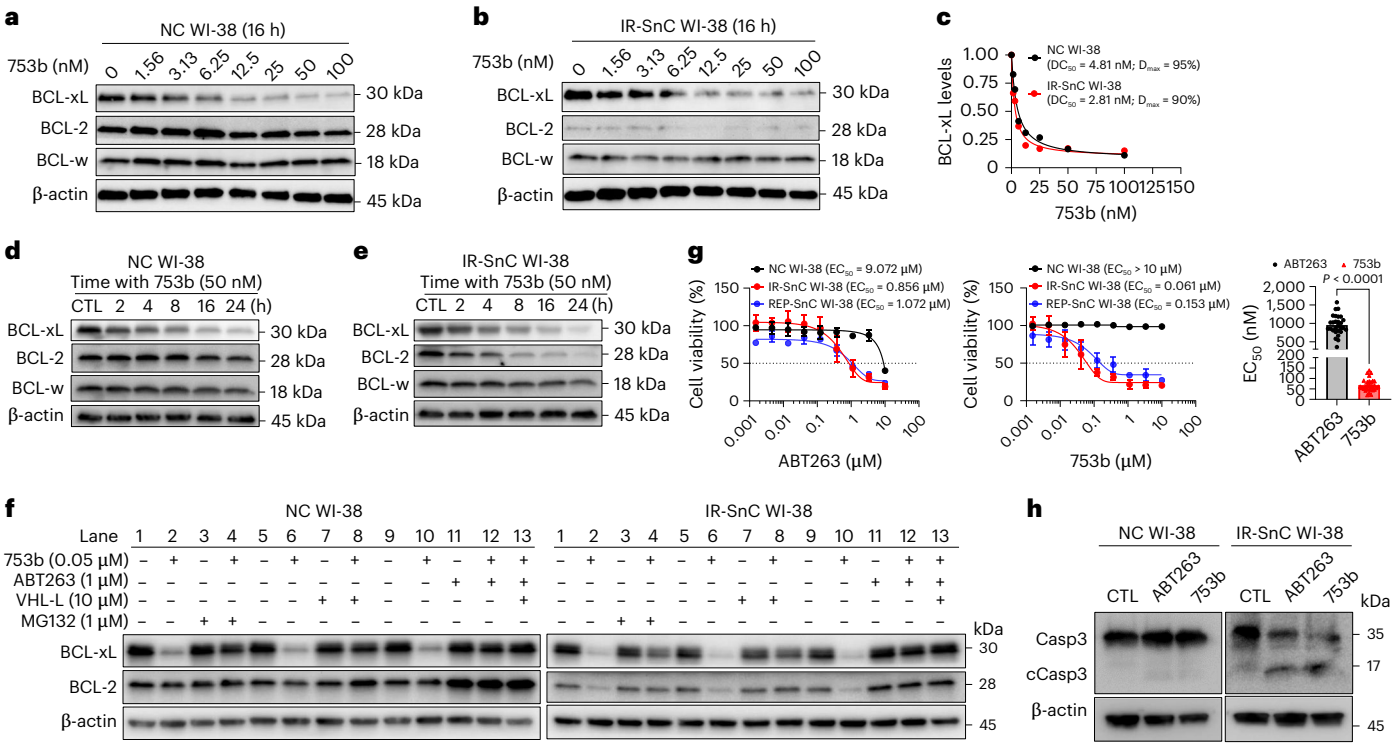

Fig. 1 | 753b is a potent and broad-spectrum senolytic agent in vitro. a,**b**, 753b degraded BCL-xL in NC and IR-SnC WI-38 cells in a dose-dependent manner. **c**, Densitometric analyses of BCL-xL expression in NC and IR-SnC WI-38 cells. Data are presented as mean from two independent assays. DC_{50}, drug concentration causing 50% degradation of protein of interest; D_{max}, the maximum level of degradation of protein of interest. **d**,**e**, 753b degraded BCL-xL in NC and BCL-xL and BCL-2 in IR-SnC WI-38 cells in a time-dependent manner. Data presented are from one experiment. Similar results were observed in a repeat. **f**, Treatment with MG132 (a 26S proteasome inhibitor), VHL-L or ABT263 2 h before 753b treatment abrogated the degradation of BCL-xL in NC (left) and BCL-xL and BCL-2 in IR-SnC (right) WI-38 cells. Data presented are from one experiment. Similar results were observed in a repeat. **g**, 753b is more potent to kill IR-SnC and REP-SnC WI-38 cells but less toxic to NC WI-38 cells than ABT263. The data presented in the left and middle panels are mean ± s.d. (left panel: $n = 6$, 6 and 3 technical replicates for NC, IR-SnC and REP-SnC, respectively; middle panel: $n = 3$, 6 and 4 technical replicates for NC, IR-SnC and REP-SnC, respectively) of a representative assay out of three independent assays, and data on the right panel are mean ± s.e.m. of multiple independent assays ($n = 28$ and 30 biological replicates for ABT263 and 753b, respectively). A two-tailed, unpaired Student's *t*-test was used. **h**, ABT263 and 753b induce apoptosis in IR-SnC WI-38 cells but not in NC WI-38 cells, as evidenced by immunoblot analysis of Caspase 3 (Casp3) activation/cleavage. Data presented are from one experiment. cCasp3, cleaved Casp3.

Furthermore, mice treated with 753b showed no significant changes in their body weight, liver weight and the ratio of liver weight to body weight and had no obvious pathology noted at autopsy (Fig. 2c). These findings indicate that 753b is relatively safe to mice.

We next examined whether 753b could clear SnCs in various tissues in naturally aged mice by measuring the expression of *Cdkn2a* (*p16*) mRNA and the SASP. We found that aged mice exhibited significant increases in the expression of *Cdkn2a* mRNA in the liver, spleen, lung, kidney and fat tissues (Fig. 2d and Extended Data Fig. 2a). Interestingly, 753b treatment significantly decreased the expression of *Cdkn2a* mRNA in the liver and spleen but not in the lung, kidney and fat tissues. 753b treatment also reduced the mRNA levels of several SASP factors in the liver, including *Il1b* and *Serpine1* but not others (Fig. 2e and Extended Data Fig. 2b). 753b also reduced the SASP in the spleen, including *Il1b*, *Serpine1*, *Mmp3*, *Cxcl12*, *Il6*, *Tnfa* and *Tnfsf11* (*Rankl*) (Extended Data Fig. 3). Moreover, liver senescence-associated beta-galactosidase (SA-β-gal) staining showed a dramatic reduction in the 753b-treated aged group (Fig. 2f,g). These results indicate that 753b can effectively reduce the SnC burden in these mice but in a tissue-selective manner.

The finding that 753b can selectively clear SnCs in naturally aged mice in a tissue-specific manner is intriguing because it is capable of killing various SnCs from different tissues except senescent PACs in vitro (Fig. 1g and Extended Data Fig. 1d–f). To gain more insights into its tissue specificity, we conducted pharmacokinetic (PK) and tissue distribution studies for 753b. We found that 753b had a long half-life in plasma and could produce good systemic levels after IP injection (Supplementary Fig. 1 and Supplementary Table 1). Interestingly, 753b exhibited a tissue-specific distribution after IP injection (Fig. 2h). The liver and spleen accumulated much higher levels of 753b for a long duration than the lung, kidney and fat tissues, which might partially explain why 753b can more effectively clear SnCs in the liver and spleen than other tissues examined. The mechanisms by which 753b is enriched in the liver and spleen have yet to be elucidated. The lack of senolytic effect of 753b on fat tissues is likely attributable to the insensitivity of senescent PACs to BCL-xL and BCL-2 targeting agents (Extended Data Fig. 1f) because senescent PACs are not dependent on BCL-xL and BCL-2 for survival[16,31].

753b effectively kills senescent murine hepatocytes in vitro

Because accumulation of senescent hepatocytes was implicated in the pathogenesis and progression of MASLD, the finding that 753b is likely a liver-tropic senolytic encouraged us to explore whether 753b can effectively kill senescent hepatocytes and has the potential to be used as a therapeutic to treat MASLD and to reduce MASH-driven HCC. We used AML-12 cells, an immortal mouse hepatocyte cell line, as an in vitro model to study the hepatic senolytic activity of 753b in comparison to ABT263. AML-12 cells became senescent after exposure to IR. The senescent AML-12 cells induced by IR exhibited typic morphological changes, reduced synthesis of DNA and cell proliferation (reduced 5-ethynyl-2′-deoxyuridine (EdU) staining), stained positive for SA-β-gal

https://doi.org/10.1038/s43587-025-00811-7

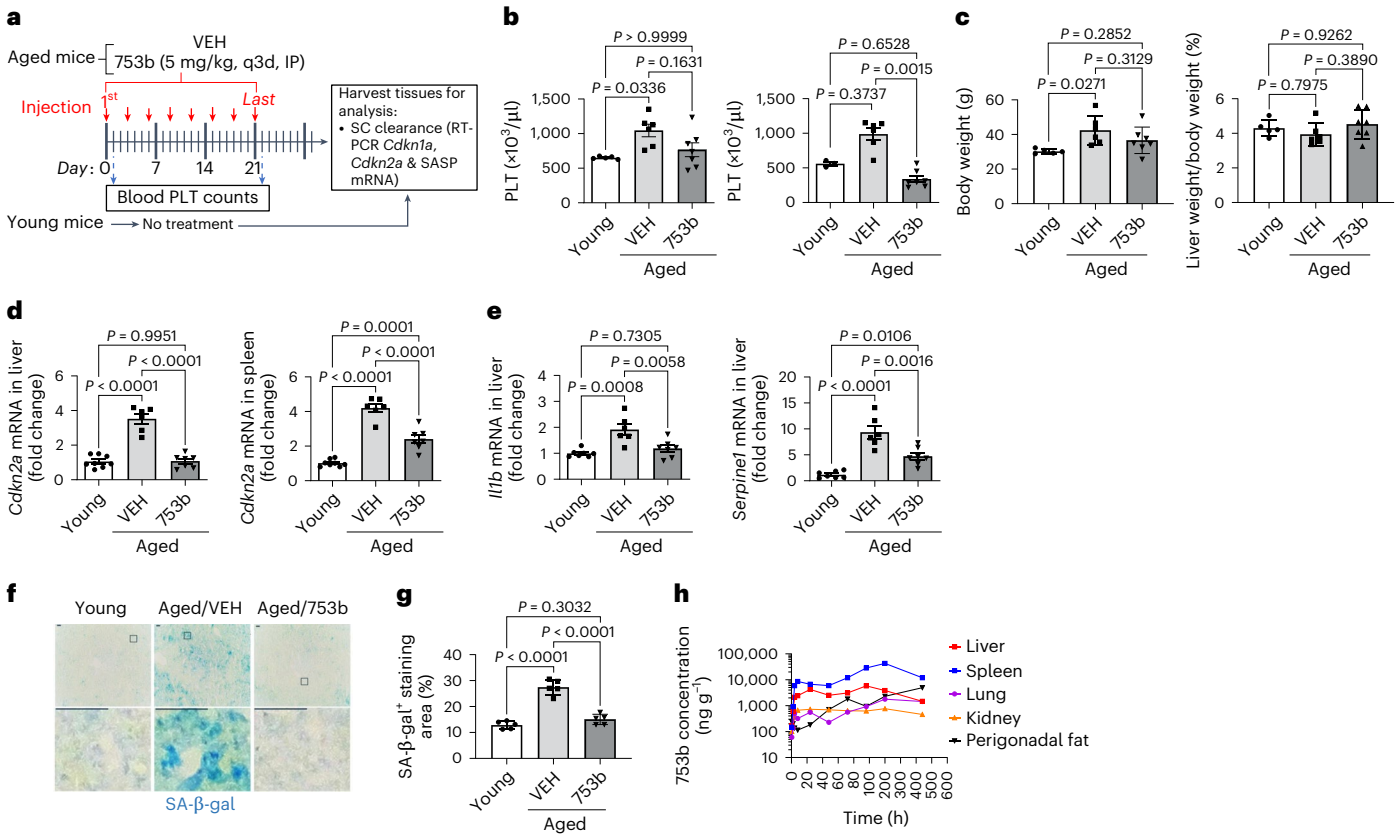

Fig. 2 | 753b effectively reduces senescence burden in naturally aged mice in a tissue-specific manner. a, The scheme of the experimental design. **b**, Blood platelet (PLT) counts in 753b-treated and vehicle (VEH)-treated aged mice 24 h after the first (left) and last (right) treatment and in control young mice. **c**, Whole body weight and the liver weight as a percentage of the whole body weight in young and VEH-treated and 753b-treated aged mice were measured at the endpoint of study. **d**, The levels of *Cdkn2a* mRNA in the liver and spleen from young and VEH-treated and 753b-treated aged mice. **e**, The levels of *Il1b* and *Serpine1* mRNA in the liver from young and VEH-treated and 753b-treated aged mice. **f**, Representative SA-β-gal staining (blue color) images of liver tissue sections from young and VEH-treated and 753b-treated aged mice (scale bar, 300 μm) (top panels) and a higher magnification of the selected areas from the top panels (lower panels). **g**, Percentage of SA-β-gal staining areas in the liver tissue sections from young and VEH-treated and 753b-treated aged mice. **h**, The mean concentrations of 753b in the liver, spleen, lung, kidney and perigonadal fat tissues of mice ($n = 2$) were monitored over 168 h after a single IP administration of 5 mg kg^{-1} 753b. The data presented in **b** are means ± s.e.m. and were analyzed by Krustal–Wallis one-way ANOVA with Dunn's post hoc test; the data presented in **c**–**e** and **g** are means ± s.e.m. and were analyzed by one-way ANOVA with Sidak's multiple comparisons test or Tukey's multiple comparisons test. For **b** and **c**, $n = 5$, 6 and 7 mice per group for young, VEH and 753b groups, respectively, except $n = 3$ for young on the right panel of **b**; for **d**, $n = 8$, 6 and 7 mice per group for young, VEH and 753b groups, respectively; for **e**, $n = 7$, 6 and 7 mice per group for young, VEH and 753b groups, respectively; and for **g**, $n = 5$ mice per group for young, VEH and 753b groups, respectively.

and expressed increased levels of mRNA for *Cdkn2a*, *Cdkn1a* and several SASP factors (*Ccl2*, *Tnfa*, *Il1b*, *Serpine1*, *Cxcl12*, *Mmp3*, *Tgfb1* and *Il6*) (Fig. 3a–c). Although non-senescent AML-12 cells were insensitive to ABT263 and 753b, the cells became highly sensitive to ABT263 and 753b after they underwent senescence (Fig. 3d). In addition, 753b is approximately two-fold more potent than ABT263 in killing senescent AML-12 cells. The cytotoxicity of 753b to senescent AML-12 cells is primarily attributable to BCL-xL degradation (Fig. 3e). Degradation of BCL-w, but not BCL-2, might partially contribute to the senolytic activity of 753b in AML-12 cells. These results confirm that 753b is senolytic to mouse senescent hepatocytes.

753b reduces SnCs and hepatic steatosis/fibrosis in mice

STAM mouse is a well-established animal model that recapitulates the human MASLD progression from hepatic steatosis to MASH, fibrosis and HCC[29,30]. STAM mice manifest hepatic steatosis and MASH around 5 weeks and 8 weeks, respectively, which progresses to fibrosis around 12 weeks, and finally develop HCC with 100% penetrance around 20 weeks[29,30]. Our preliminary studies revealed that the disease progression in STAM mice was associated with an increased accumulation of SA-β-gal$^+$ senescent periportal hepatocytes that were positive for hepatocyte nuclear factor 4α (HNF4α) and glucose-6-phosphatase-α (G6Pα) staining (Extended Data Fig. 4a–d). In contrast, no significant SA-β-gal staining was found in pericentral hepatocytes that express the cytochrome P450 enzyme (Cyp2E1) and CK19$^+$ bile duct epithelial cells (Extended Data Fig. 4b,e). These findings are in agreement with previously reported findings[8,33], suggesting that periportal hepatocytes are more susceptable to metabolic stress-induced senescence than hepatocytes in the other hepatic zones, and MASLD progression in STAM mice was associated with an increase of senescence in G6Pα$^+$ and HNF4α$^+$ periportal hepatocytes. To determine the role of senescent hepatocytes as well as other types of SnCs in the liver in the progression of MASLD from hepatic steatosis to MASH, liver fibrosis and HCC and to evaluate the therapeutic potential of 753b for the disease, we established a STAM mouse model by injecting a single dose of STZ into P2 C57BL/6 mice, followed by an HFD from P30 to the end of the experiment on P150 (ref. 29). On P45, half of the STAM mice were treated with vehicle, and the other half was given 753b twice a week at 5 mg kg^{-1} via IP injection until the end of the experiment (Fig. 4a). A small number of mice were euthanized on P90 to evaluate SnC clearance and hepatic steatosis, and the rest of the mice were euthanized on P150 to evaluate SnC clearance, hepatic fibrosis and HCC. 753b treatment significantly

https://doi.org/10.1038/s43587-025-00811-7

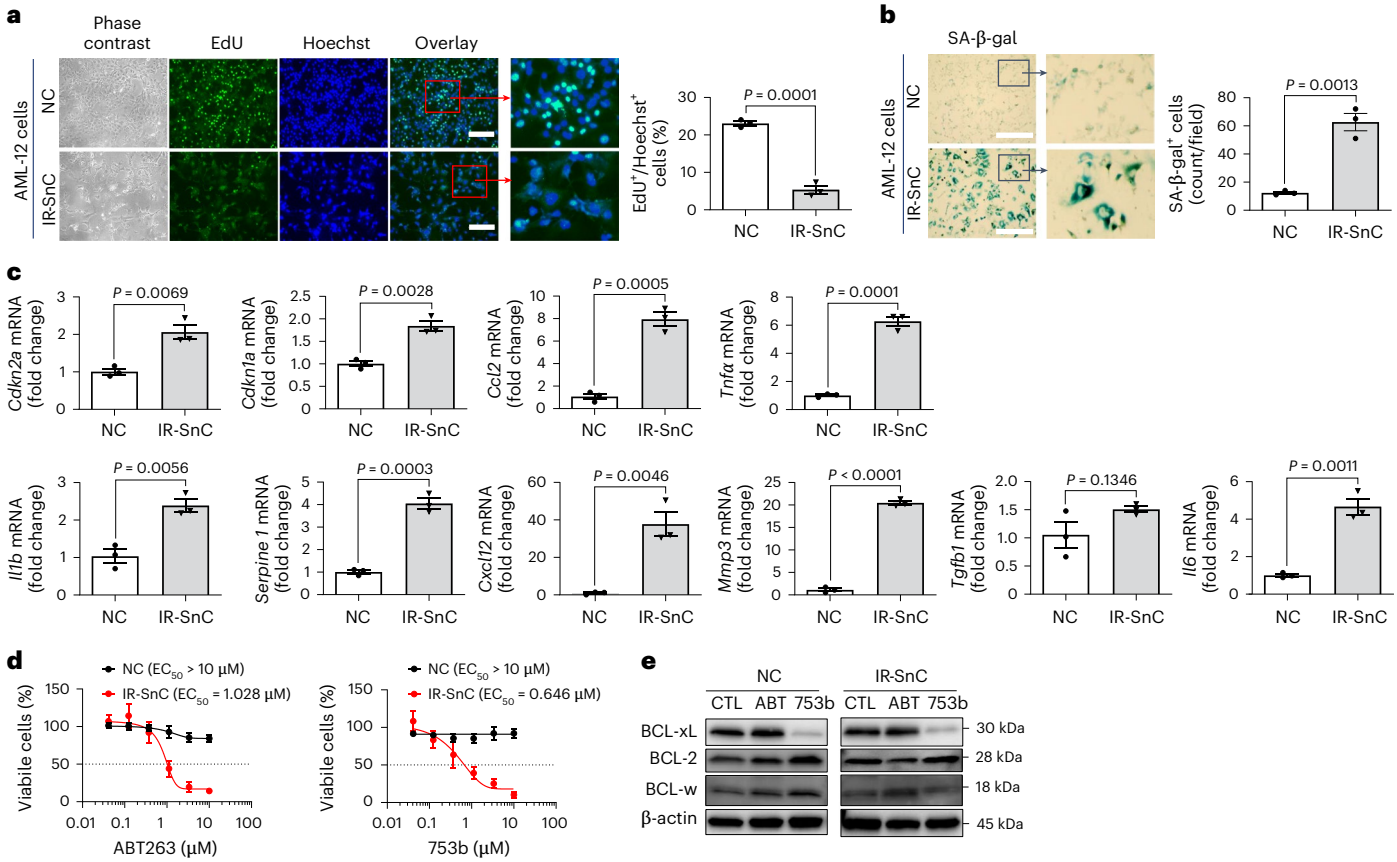

Fig. 3 | 753b is a more potent senolytic than ABT263 against senescent murine hepatocytes. a, Representative images of phase contrast, EdU stainig, nuclear staining with Hoechst 33342 (Hoechst) and the overlays of these two stainings of NC and IR-SnC AML-12 cells (scale bar in the overlay, 300 μm) and images of a higher magnification of the selected areas from the overlay images are shown on the left, and percentages of EdU$^+$/Hoechst$^+$ cells are shown on the right. **b**, Representative images of SA-β-gal staining of NC and IR-SnC AML-12 cells (scale bar, 300 μm) and images of a higher magnification of the selected areas from the SA-β-gal staining images are shown on the left, and percentages of SA-β-gal$^+$ cells are shown on the right. **c**, The levels of *Cdkn2a*, *Cdkn1a*, *Ccl2*, *Tnfa*, *Il1b*, *Serpine1*, *Cxcl12*, *Mmp3*, *Tgfb1* and *Il6* mRNA in NC and IR-SnC AML-12 cells. **d**, 753b is more potent against IR-SnC AML-12 cells than ABT263. The data presented are mean ± s.d. ($n = 6$ technical replicates) of a representative assay. Similar results were observed in two more independent assays. **e**, Representative immunoblot images show that treatment with 753b (0.3 μM), but not ABT263 (0.3 μM), can degrade BCL-xL in NC AML-12 cells and BCL-xL and BCL-w in IR-SnC AML-12 cells. The data presented in all the bar graphs are means ± s.e.m. ($n = 3$ independent assays) and were analyzed by a two-tailed, unpaired Student's *t*-test.

reduced liver SA-β-gal staining and mRNA expression for *Cdkn2a* and *Cdkn1a* (Fig. 4b,c and Extended Data Fig. 4f). This reduction was associated with a decreased expression of BCL-xL, suggesting that 753b can effectively clear SnCs in the livers of STAM mice via degradation of BCL-xL (Fig. 4d).

Next, we examined whether 753b treatment can reduce hepatic steatosis and fibrosis in STAM mice. We found that the areas of Oil Red O staining and levels of hepatic triglyceride in the livers from 753b-treated mice were significantly reduced in comparison to vehicle-treated STAM mice (Fig. 4e,f). More importantly, 753b treatment also reduced the expression of several fibrosis-related markers, including alpha-smooth muscle actin (*αSMA* or *Acta2*), connective tissue growth factor (*Ctgf* or *Ccn2*), type I pro-collagen (*Col1A1*), transforming growth factor-β1 (*Tgfb1*) and platelet-derived growth factor-β (*Pdgfb*) at the level of transcription (Fig. 4g). This reduction was associated with a significant decrease in the expression of mRNA for several SASP inflammatory factors (such as *Ccl2* and *Ccl5*) and genes regulating necroptosis (*Mlkl* and *Ripk3*) and macrophage activation (*Cd68* and *Itgax* or *Cd11c*), which are known to play an important role in MASH and liver fibrosis via induction of chronic inflammation, necroptosis and tissue fibrosis (Extended Data Fig. 4g)[34–38]. Moreover, 753b administration nearly diminished myofibroblast activation as revealed by western blotting of the cell-specific marker αSMA, and collagen deposition was significantly lower in 753b-treated mouse livers than those after vehicle treatment, as shown by the Sirius Red staining and western blot analysis (Fig. 4h,i). Decreased hepatic fibrosis after 753b treatment was further verified by quantitative measurement of collagen content in the livers based on hydroxyproline assay (Fig. 4j). The reduction of liver SnCs and hepatic steatosis and fibrosis was associated with a significant improvement in the liver function in STAM mice after 753b treatment (Fig. 4k). Collectively, these results demonstrate that 753b treatment can effectively reduce hepatic steatosis and fibrosis in STAM mice, at least in part via clearance of SnCs. Moreover, the mice treated with 753b exhibited a healthier phenotype without significant changes in body weight and with a better response to insulin in an insulin tolerance test (ITT) (Extended Data Fig. 4h–j).

753b reduces HCC in STAM mice in a time-dependent manner

To determine the effect of clearing hepatic SnCs with 753b on HCC development in STAM mice, we performed magnetic resonance imaging (MRI) to determine the number and volume of liver lesions 3 d before the end of the experiment (Fig. 4a). Abdominal MRI examinations detected obvious large HCC lesions in vehicle-treated mice, whereas few and smaller lesions were found in 753b-treated mice (Fig. 5a). Specifically, T1-weighted pre-contrast injection and T2-weighted Gd-chelate-enhanced MRI demonstrated cancer tissues that were

https://doi.org/10.1038/s43587-025-00811-7

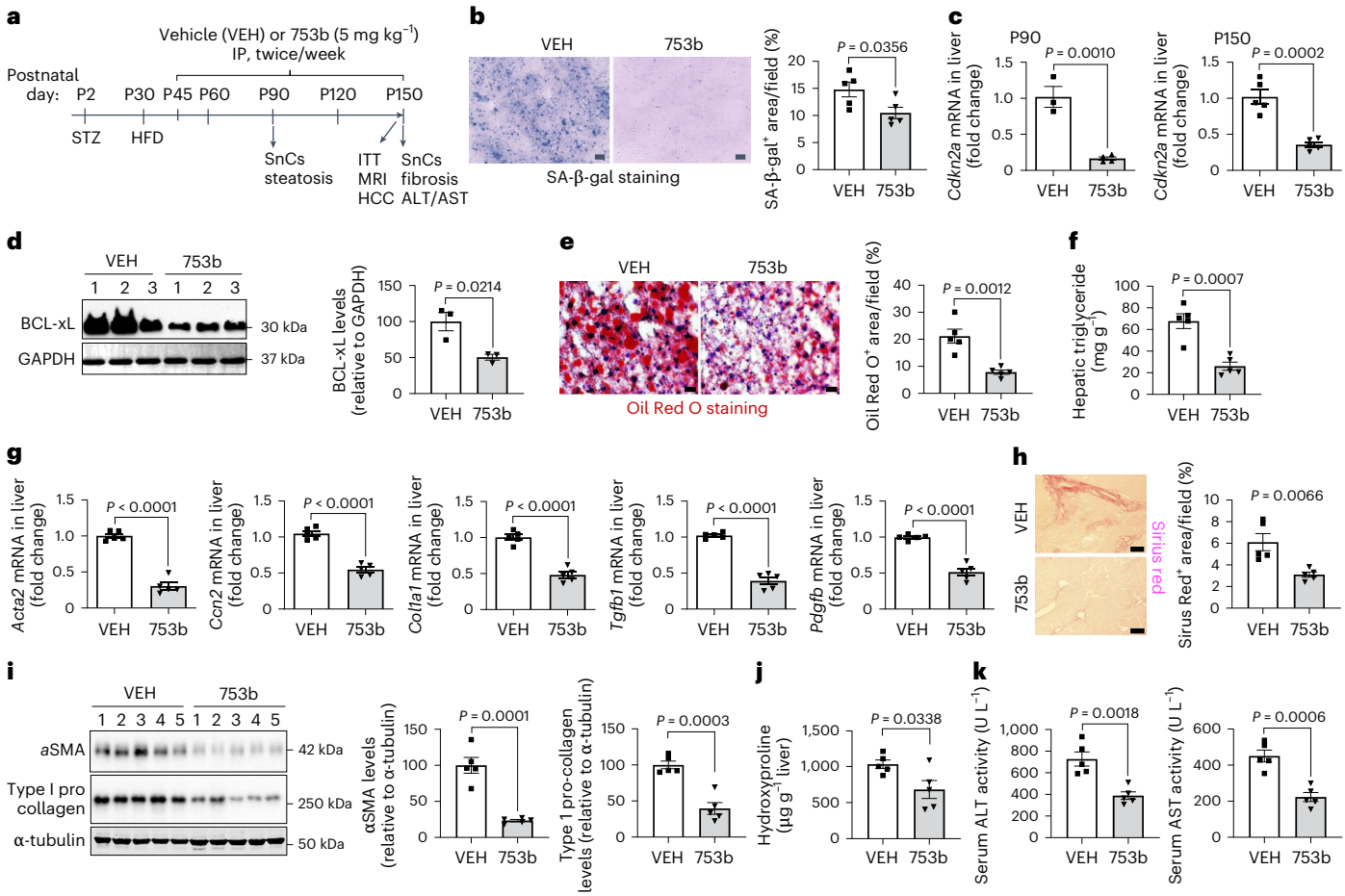

Fig. 4 | 753b reduces hepatic cellular senescence, steatosis, fibrosis and injury in STAM mice. a, Experimental design. 753b, 753b-treated STAM mice; VEH, vehicle-treated STAM mice. **b**, Representative images of SA-β-gal staining (dark blue color) (left panel) and percentage of SA-β-gal staining areas in the liver tissues from mice on P90. Scale bar, 150 μm. **c**, The levels of *Cdkn2a* mRNA in the tumor-free liver tissues from mice on P90 and P150. **d**, Western blot images (left) and densitometric quantification (right) of the BCL-xL levels in the livers from mice on P150. **e**, Representative Oil Red O staining images (left panels) and quantification (right panel) of the percentage of areas with the staining in the images of the livers from STAM mice on P90. Scale bar, 50 μm. **f**, The levels of triglyceride in the livers on P90. **g**, The relative expression of selective fibrosis-related genes in the tumor-free liver tissues from STAM mice on P150. **h**, Representative Sirius Red staining (left panels) and the quantification of the staining in the tumor-free liver tissues from STAM mice on P150. Scale bars, 200 μm. **i**, Western blotting images (left panel) of αSMA and type I pro-collagen in the tumor-free liver tissues from STAM mice on P150. The levels of αSMA (middle panel) and type I pro-collagen (right panel) relative to the levels of α-tubulin were quantified by densitometry. **j**, The levels of hydroxyproline in the tumor-free liver tissues from STAM mice on P150. **k**, The serum levels of ALT and AST from STAM mice on P150. Data presented in all the bar graphes are means ± s.e.m. ($n = 5$ mice per group) except in the left panel of **c** ($n = 3$ mice for the VEH group and $n = 4$ mice for the 753b group) and **d** ($n = 3$ mice per group) and were analyzed by a two-tailed, unpaired Student's *t*-test.

hypointense in T1 and hyperintense in T2, respectively. These MRI signals matched morphological evaluations and histological inspections of the livers from the euthanized animals (Fig. 5b). Furthermore, quantitation of the number of tumor nodules and tumor volume in the livers confirmed that 753b administration significantly reduced the development of HCC in STAM mice compared to vehicle treatment (Fig. 5c), which was associated with a reduced ratio of liver to body weight (Fig. 5d). Moreover, western blotting analysis for the liver cancer marker glypican 3 (Gpc3) showed that 753b administration significantly reduced the liver expression of Gpc3 in STAM mice compared to vehicle treatment (Fig. 5e). Collectively, all these results suggest that 753b can effectively inhibit HCC development in STAM mice.

Because STAM mice develop hepatic steatosis, MASH, fibrosis and HCC in a highly predictable and time-dependent manner[29,30], we next examined if the timing affects the ability of 753b treatment to inhibit HCC development in the STAM model by varying the time for the initiation and termination of 753b treatment either during hepatic steatosis and early stage of steatohepatitis (that is, from P45 to P90, termed early treatment) or between MASH/fibrosis and early onset of HCC development (that is, from P90 to P150, termed delayed treatment) (Extended Data Fig. 5). We found that early treatment with 753b did not significantly reduce SnC accumulation in the liver at the end of the experiment on P150 based on changes in SA-β-gal staining and expression of *Cdkn1α* mRNA but not *Cdkn2α* mRNA that was slightly reduced after 753b treatment (Fig. 6a–c). This early treatment also had no significant effect on the progression of MASLD from hepatic steatosis, MASH and fibrosis to HCC (Fig. 6d–h). In addition, early treatment also failed to reduce liver damage based on the analysis of alanine transaminase (ALT) and aspartate transaminase (AST) levels (Fig. 6i), which was associated with no significant changes in the markers for liver inflammation (such as expression of *Ccl2* and *Ccl5* mRNA) but a slight increase in the markers of necroptosis (*Mlkl* and *Ripk3*) and macrophage activation (*Itgax*) (Extended Data Fig. 6a). In contrast, the delayed treatment significantly reduced liver SnC accumulation, steatosis, fibrosis and HCC (Fig. 7a–i and Extended Data Fig. 6b), which led to a significant reduction in liver damage (Fig. 7j). These changes

https://doi.org/10.1038/s43587-025-00811-7

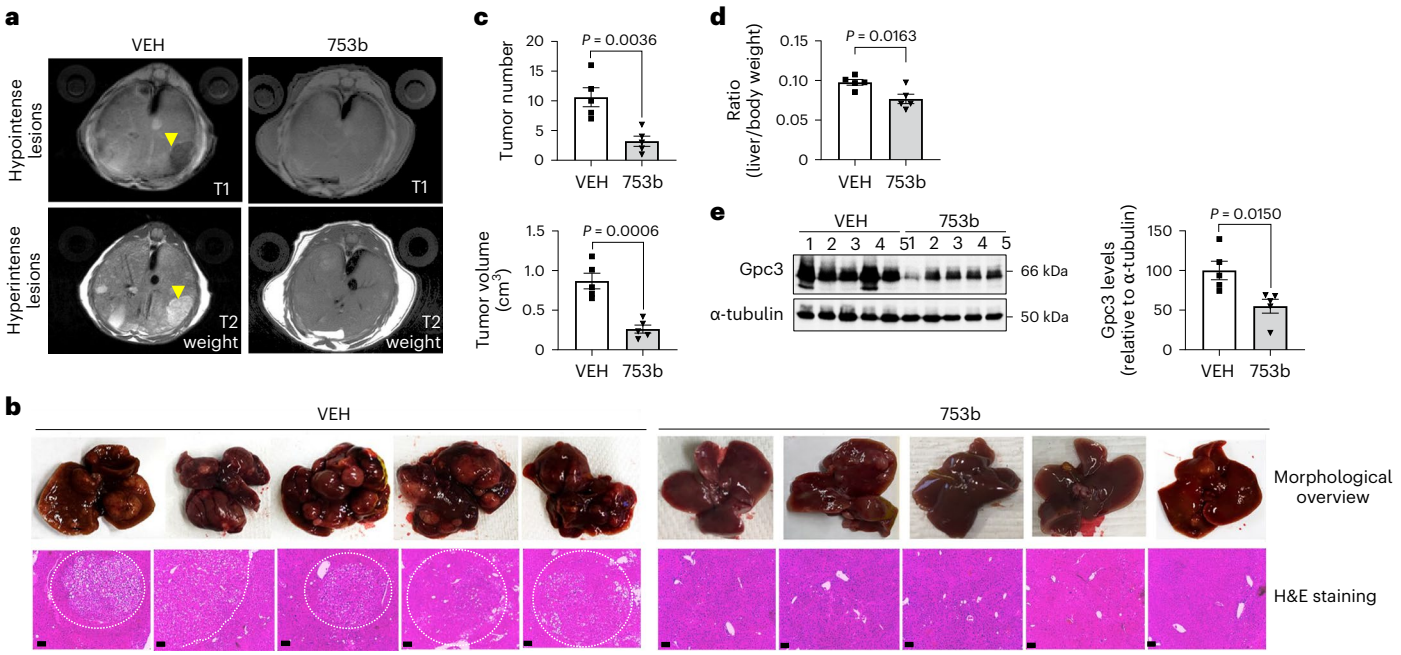

Fig. 5 | 753b administration reduces tumorigenesis in STAM mice. **a**, Representative MRI T1 pre-contrast and T2-weighted images of vehicle (VEH)-treated and 753b-treated STAM mice. Tumor lesions (indicated by yellow arrows) were determined based on hypointense signals in T1 and hyperintense signals in T2-weighted images. **b**, Images of morphological overviews (upper panel) of the whole livers and representative microscopic images (lower panel) of the H&E staining of the liver tissues from five VEH-treated and 753b-treated STAM mice. Tumors in the lower panel are circled by the white dotted lines. Scale bar, 150 µm. **c**, The number (upper panel) and volume (lower panel) of HCC lesions were quantified according to the MRI T1 and T2-weighted images. Data for each mouse were analyzed based on 5–6 slices of images that covered the whole liver lobes. **d**, The ratios between liver and body weight of VEH-treated and 753b-treated STAM mice. **e**, Gpc3 expression in the liver tissues from VEH-treated and 753b-treated STAM mice was measured by western blotting (left panel) and quantified by densitometry (right panel). Data presented in all the bar graphes are means ± s.e.m. ($n = 5$ mice per group) and were analyzed by a two-tailed, unpaired Student's t-test. MRI assays were done 3 d before the termination of the study on P150, and all other assays were done on P150. H&E, hematoxylin and eosin.

were also associated with a significant reduction in the expression of several SASP factors and markers of liver necroptosis (*Mlkl* and *Ripk3* mRNA) and macrophage activation (*Itgax* mRNA) (Extended Data Fig. 6c). These findings suggest that 753b is capable of inhibition of HCC development in STAM mice even after MASH has been developed. In addition, it is suggestive that continuous accumulation of SnCs during MASH/fibrosis is important for promoting HCC development.

Because 753b is a dual BCL-xL and BCL-2 degrader that has anti-tumor activity by inducing apoptosis in tumor cells with dependence on BCL-xL and/or BCL-2 (refs. 39,40), we next investigated whether its anti-tumor activity might contribute to its inhibition of HCC development in STAM mice. First, we further delayed the initiation of 753b treatment in the STAM mice on P145 when HCC presumably had already developed (Fig. 8a and Extended Data Fig. 5). We found that this further delayed or later treatment had no effect on HCC development and progression (Fig. 8b,c). Furthermore, we established an oncogene-induced HCC mouse model by the hydrodynamic tail vein injection (HTVi) of plasmids expressing c-MET, a mutated β-catenin (β-Cat) called ΔN90-β-catenin and Sleeping Beauty transposon in FVB/NJ mice[41]. After the mice developed HCC based on increased blood levels of alpha-fetoprotein (AFP), we started the treatment of the mice with vehicle or 753b 4 weeks after HTVi for 5 weeks and then examined the progression of HCC in the mice by measuring the blood levels of AFP and inspected HCC development at the end of the experiment (Fig. 8d). We found that 753b did not inhibit HCC progression (Fig. 8e,f). Collectively, these findings suggest that 753b has no direct anti-tumor activity against HCC cells, probably because they are not dependent on BCL-xL and BCL-2 for survival. To test this hypothesis, we examined the effects of ABT263 and 753b on two widely used HCC cell lines, HepG2 and Huh7 cells, in vitro. We found that neither 753b nor ABT263 was cytotoxic to HepG2 and Huh7 cells, even though 753b could potently degrade BCL-xL and BCL-2 in the cells (Extended Data Fig. 7). This finding, along with the discovery that 753b can effectively clear SnCs and reduce liver steatosis and fibrosis, implies that 753b inhibits HCC development in STAM mice primarily via its senolytic activity.

Discussion

Here we report the discovery of a tissue-selective senolytic agent, 753b. We found that 753b could potently kill SnCs derived from several different tissue origins in vitro via degrading BCL-xL as well as BCL-2, including senescent fibroblast cells, renal epithelial cells and endothelial cells, with the exception of senescent PACs that are known to be independent BCL-xL and BCL-2 for survival[16,31]. However, in naturally aged mice, 753b administration cleared SnCs selectively in the liver and spleen but not in the lung, kidney and fat tissues. This tissue selectivity is likely in part attributable to its selective tissue distribution because the liver and spleen accumulated much higher levels of 753b over a long duration than the lung and kidney tissues after its administration. In addition, differences in the sensitivity of SnCs from different tissue origins to 753b may also contribute to this tissue selectivity because senescent hepatocytes, but not senescent PACs, are very sensitive to 753b. The mechanisms by which 753b is enriched in the liver and spleen have yet to be investigated. However, it is suggestive that the differential tissue distribution of a senolytic can be exploited to achieve tissue-selective clearance of SnCs.

Tissue-selective senolytics may offer some advantages over pan-senolytics as potential therapeutics for diseases caused by SnC accumulation. It has been shown that not all SnCs are bad neighbors, because some of them also play important roles in physiology[42,43], including organogenesis during fetal development[44,45] and promotion

https://doi.org/10.1038/s43587-025-00811-7

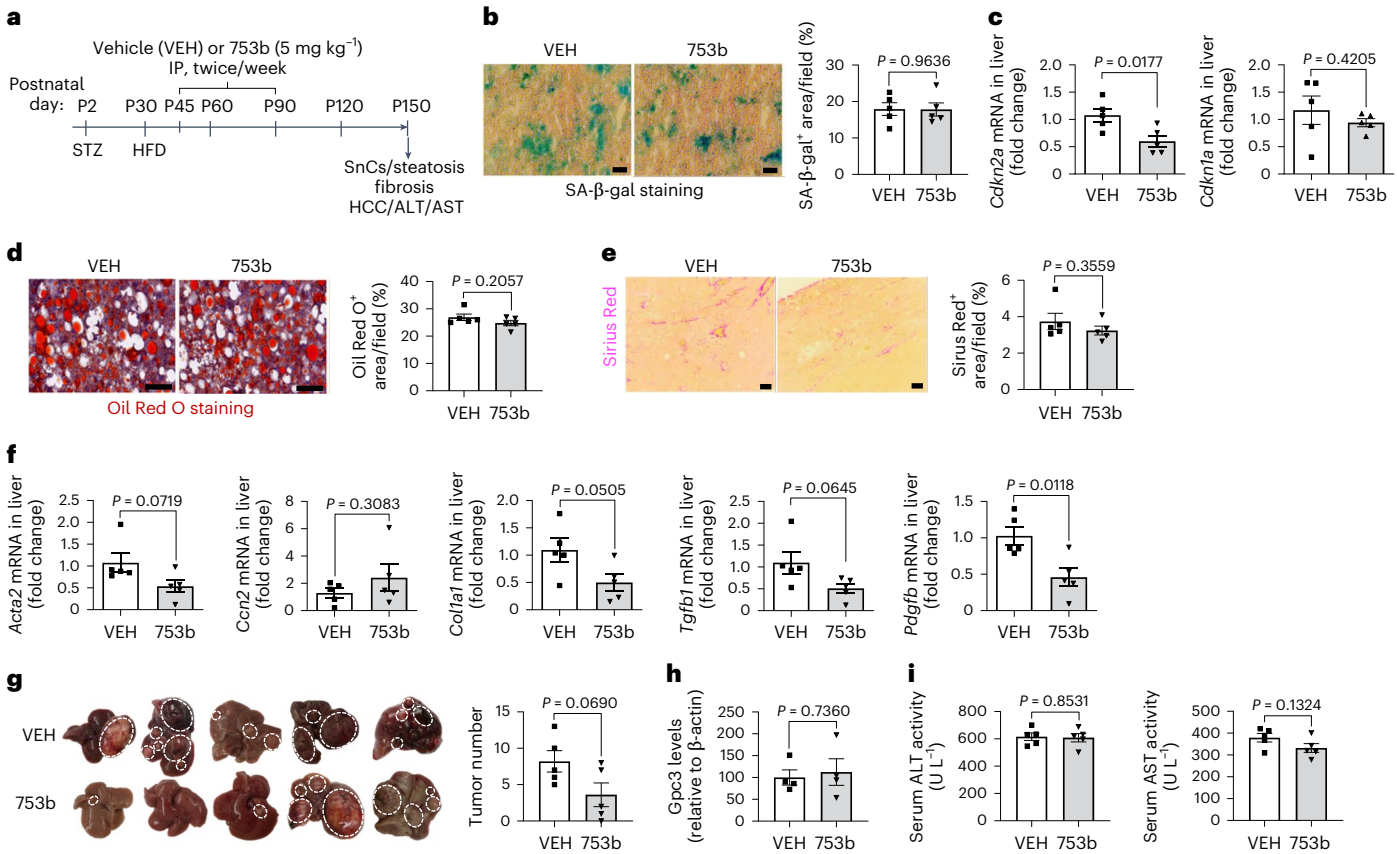

Fig. 6 | Early treatment (P45–P90) with 753b has no effect on hepatic cellular senescence, steatosis, fibrosis and injury and on HCC development in STAM mice. a, Diagram illustrating the experimental design for the early 753b treatment. **b**, Left, representative images of SA-β-gal staining (green color) in the liver tissues from vehivle (VEH)-treated and 753b-treated STAM mice. Scale bar, 150 μm. Right, percentage of SA-β-gal staining areas in the liver tissue sections from VEH-treated and 753b-treated STAM mice. **c**, The levels of *Cdkn2a* and *Cdkn1a* mRNA in the tumor-free liver tissues from VEH-treated and 753b-treated STAM mice. **d**, Representative Oil Red O staining images (left panels) and quantification (right panel) of the percentage of areas with Oil Red O staining in the images of the livers from VEH-treated and 753b-treated STAM mice. Scale bar, 150 μm. **e**, Representative Sirius Red staining (left panels) and the quantification of the staining in the tumor-free liver tissues from VEH-treated and 753b-treated STAM mice. Scale bars, 200 μm. **f**, The relative expression of selective fibrosis-related genes in the tumor-free liver tissues from VEH-treated and 753b-treated STAM mice. **g**, Left, images of morphological overviews of the whole livers from VEH-treated and 753b-treated STAM mice. Tumors in the images are circled by the white dotted lines. Right, the number of HCC lesions as seen on the left images. **h**, Gpc3 expression in the liver tissues from VEH-treated and 753b-treated STAM mice was measured by western blotting and quantified by densitometry. **i**, The serum levels of ALT and AST from VEH-treated and 753b-treated STAM mice. Data presented in all the bar graphes are means ± s.e.m. ($n = 5$ mice per group) except in **h** ($n = 4$ mice per group) and were analyzed by a two-tailed, unpaired Student's *t*-test. All the assays were done on P150.

of tissue damage repair[46]. Recently, a population of p16-expressing fibroblasts was discovered in the basement membrane adjacent to epithelial stem cells in the mouse lung[47]. These cells exhibit some SnC phenotypes and express SASP factors after injury. However, the expression of SASP factors by these cells can promote epithelial stem cell regeneration and epithelial repair in the lung. In addition, with more advanced age, when tissues have exhausted their regenerative capacity, SnCs may still play some roles in maintaining tissue integrity and functionality. For example, increased expression of p16 induces senescence in pancreatic β cells[48]. These p16-expressing β cells secrete increased levels of insulin, which may help to maintain glucose homeostasis by compensating for the age-dependent loss of β cells. Therefore, non-specific clearance of SnCs with a pan-senolytic may carry some health risks by delaying wound healing after tissue injury and surgery and even disrupting normal tissue integrity and homeostasis in some older adults. These risks can be mitigated by the use of senomorphics that can inhibit the expression of SASP factors without killing SnCs[13]. Alternatively, a tissue-selective senolytic such as 753b can also be useful by selectively clearing SnCs in a disease-affecting tissue to reduce the risks. However, the drawback of tissue-selective senolytics is that they would be less effective than pan-senolytics in preventing and/or treating multiple diseases associated with SnC accumulation during aging.

Accumulating evidence suggests that cellular senescence plays an important role in the pathogenesis and progression of MASLD during aging as well as with obesity and diabetes. Aging and lipid accumulation induce hepatocyte senescence[8,33], which, in turn, reduces hepatocyte insulin sensitivity and perturbs its metabolism, suggesting that hepatocyte senescence can drive hepatic steatosis. This is supported by the finding that clearance of SnCs via a genetic strategy or the use of two widely used senolytic agents, dasatinib and quercetin (D+Q), reduced hepatic steatosis in aged mice fed with an HFD[8]. In addition, through secretion of SASP factors, senescent hepatocytes may also promote the development of MASH, liver fibrosis and HCC by activating hepatic stellate cells (HSCs) and perpetuating metabolic dysregulation in other tissues, including the pancreas and adipose tissue. In fact, 3–7% of senescent hepatocytes can occur under normal conditions, but this can increase to 50–100% in end-stage liver diseases[9]. The accumulation of senescent hepatocytes may play a critical role in the induction and progression of MASLD[8–10]. On the other hand, senescence can occur in other cell types in the liver, including HSCs[32,49], cholangiocytes[50] and liver sinusoid endothelial cells

https://doi.org/10.1038/s43587-025-00811-7

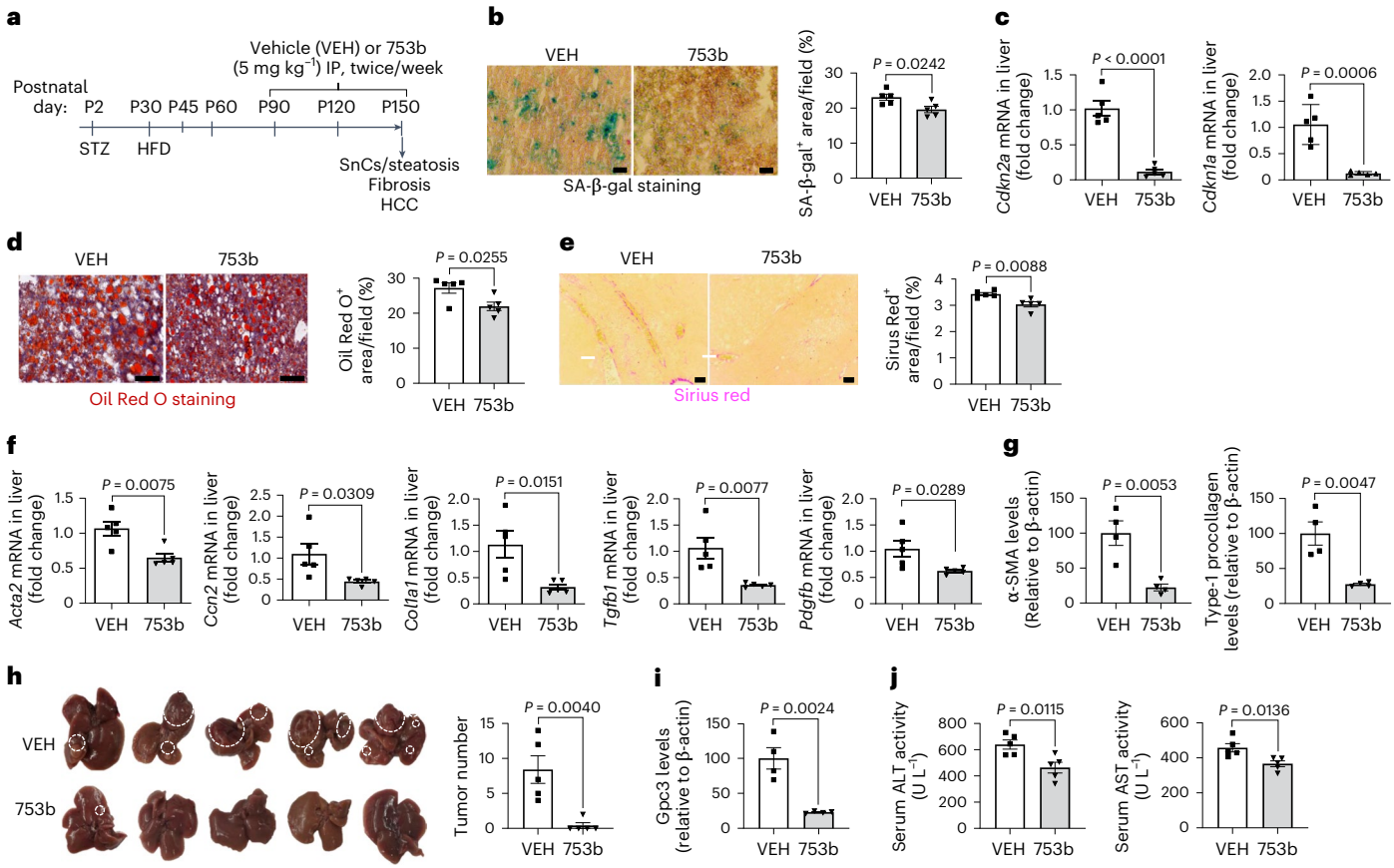

Fig. 7 | Delayed treatment (P90–P150) with 753b reduces hepatic cellular senescence, steatosis, fibrosis and injury and inhibits HCC development in STAM mice. a, Diagram illustrating the experimental design for the delayed 753b treatment. **b**, Left, representative images of SA-β-gal staining (green color) in the liver tissues from VEH-treated and 753b-treated STAM mice. Scale bar, 150 μm. Right, percentage of SA-β-gal staining areas in the liver tissue sections from VEH-treated and 753b-treated STAM mice. **c**, The levels of *Cdkn2a* and *Cdkn1a* mRNA in the tumor-free liver tissues from VEH-treated and 753b-treated STAM mice. **d**, Representative Oil Red O staining images (left panels) and quantification (right panel) of the percentage of areas with Oil Red O staining in the images of the livers from VEH-treated and 753b-treated STAM mice. Scale bar, 150 μm. **e**, Representative Sirius red staining (left panels) and the quantification of the staining in the tumor-free liver tissues from VEH-treated and 753b-treated STAM mice. Scale bars, 200 μm. **f**, The relative expression of selective fibrosis-related genes in the tumor-free liver tissues from VEH-treated and 753b-treated STAM mice. **g**, The levels of αSMA (middle panel) and type I pro-collagen (right panel) relative to the levels of β-actin were measured by western blotting and quantified by densitometry. **h**, Left, images of morphological overviews of the whole livers from VEH-treated and 753b-treated STAM mice. Tumors in the images are circled by the white dotted lines. Right, the number of HCC lesions as seen on the left images. **i**, Gpc3 expression in the liver tissues from VEH-treated and 753b-treated STAM mice was measured by western blotting and quantified by densitometry. **j**, The serum levels of ALT and AST from VEH-treated and 753b-treated STAM mice. Data presented in all the bar graphs are means ± s.e.m. ($n = 5$ mice per group except $n = 4$ for **g** and **i**) and were analyzed by a two-tailed, unpaired Student's *t*-test. All the assays were done on P150.

(LSECs)[51], during aging and under various pathological conditions. Some studies show that HSC senescence may limit the extent of liver fibrosis[32] or contribute to liver fibrosis in a different model system[52], whereas senescent cholangiocytes and LSECs may contribute to liver fibrosis by impairing liver regeneration and causing endothelial dysfunction, respectively[9,51,53]. Therefore, multiple types of liver cells may undergo senescence during the development and progression of MASLD and contribute to the development of HCC. 753b treatment in this study may clear not only senescent hepatocytes but also other potential cellular sources of SnCs in the liver. Indeed, our preliminary study showed that radiation-induced senescent LX-2 human HSCs are more sensitive to 753b than ABT263, whereas non-irradiated normal LX-2 HSCs are less sensitive to 753b and ABT263 (Supplementary Fig. 2). However, the effect of 753b on other types of senescent cells in the liver has yet to be further characterized. This collective effect of 753b on different types of SnCs may lead to the inhibition of progression of MASLD and development of HCC. However, the role of senescent hepatocytes in these pathological conditions may be context dependent, particularly considering that, in a recent study, D+Q treatment failed to clear SnCs in the liver and unexpectively exacerbated liver disease progression and tumorigenesis in an MASLD mouse model induced by diethylnitrosamine and HFD[54].

To take the advantage of the tissue-selective senolytic activity of 753b, we examined the role of SnCs in the liver in the progression of MASLD, particularly in the development of MASH-driven HCC, using a STAM mouse model that mimics the disease in human caused by diabetes and obesity. We found that 753b could more potently kill senescent hepatocytes in vitro than ABT263, and its administration effectively reduced SnCs in the livers from STAM mice. This clearance resulted in reduced hepatic steatosis and fibrosis and improved liver function and overall health of the mice. More importantly, it also reduced HCC in the mice. Because the majority of SA-β-gal$^+$ SnCs in the liver from STAM are G6Pα$^+$ and HNF4α$^+$ periportal hepatocytes, but not Cyp2E1$^+$ pericentral hepatocytes and CK19$^+$ bile duct epithelial cells, it is suggestive that senescent hepatocytes not only play a role in the induction of hepatic steatosis but also promote the progression of MASLD from steatosis to MASH, liver fibrosis and HCC in a condition mimicking the human diseases of diabetes and obesity. Therefore, 753b may inhibit the progression of MASLD and development of HCC in the STAM mice in part via clearance of senescent periportal hepatocytes.

https://doi.org/10.1038/s43587-025-00811-7

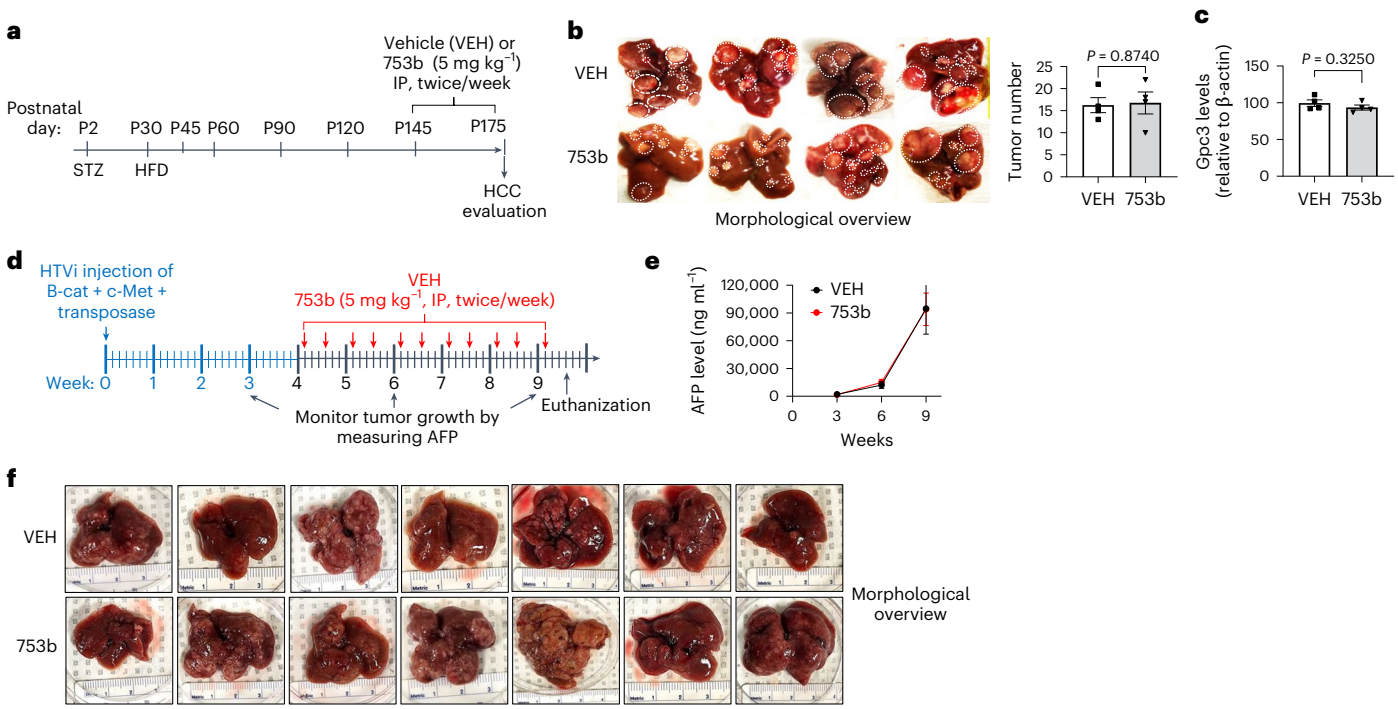

Fig. 8 | 753b dose not inhibt HCC progression. a, Diagram illustrating the experimental design for the further delayed or later 753b treatment in STAM mice. **b** Left, images of morphological overviews of the whole livers from vehicle (VEH)-treated and 753b-treated STAM mice. Tumors in the images are circled by the white dotted lines. Right, the number of HCC lesions as seen on the left images. **c**, Gpc3 expression in the liver tissues from VEH-treated and 753b-treated STAM mice was measured by western blotting and quantified by densitometry. The data presented in the bar graphs of **b** and **c** are means ± s.e.m. ($n = 4$ mice per group) and were not statistically significant analyzed by a two-tailed, unpaired Student's t-test. **d**, Diagram illustrating the experimental design for the HTVi-induced HCC with or without 753b treatment. **e**, Plasma levels of AFP in VEH-treated and 753b-treated mice after HTVi. Data presented are means ± s.e.m. ($n = 7$ mice per group). **f**, Images of morphological overviews of the whole livers from VEH-treated and 753b-treated mice.

However, it has yet to be determined whether 753b can also effectively kill senescent HSCs and other SnCs in the liver and whether clearance of these senescent cells by 753b contributes to its therapeutic efficacy against MASH-driven HCC in the STAM mouse model as well, because some of these SnCs have been implicated in the progression of MASLD in several other HCC mouse models[55,56]. Interestingly, the effects of 753b on the progression of MASLD and development of HCC in STAM mice is time dependent. Its treatment could effectively inhibit hepatic steatosis, MASH, liver fibrosis and HCC if it was given to the STAM mice between MASH/fibrosis and early onset of HCC development (that is, from P90 to P150) but was ineffective if it was given to the STAM mice during hepatic steatosis and early stage of MASH (that is, from P45 to P90) or after HCC already developed (between P145 and P175). These findings suggest that 753b is capable of inhibition of HCC development in STAM mice even after MASH has been developed but cannot inhibit HCC progression after HCC has been formed. Therefore, its effect on MASH-driven HCC is not attributable to its anti-tumor activity but, rather, to its senolytic activity. This suggestion is further supported by the finding that 753b treatment had no significant effect on the progression of HCC induced by HTVi of plasmids expressing c-MET, a mutated β-catenin (β-Cat) called ΔN90-β-catenin and Sleeping Beauty transposon in FVB/NJ mice and that 753b is not cytotoxic to HepG2 and Huh7 HCC cell lines in vitro. In addition, our findings also suggest that continuous accumulation of SnCs during MASH/fibrosis is important for promoting HCC development in the STAM model. Therefore, senolytics such as BCL-xL and BCL-2 PROTACs have the potential to be used as therapeutics to inhibit MASH progression and reduce MASH-driven HCC. However, considering that the STAM model represents a metabolic syndrome-driven MASH/HCC model caused by pancreatic damage and then exacerbated by HFD, it has yet to be determined whether 753b can also inhibit the development of HCC that is not caused by the metabolic syndrome, including alcohol-induced liver disease and chronic liver damage and inflammation for which cellular senescence has been implicated in the pathogenesis of the disease progression as well.

In summary, our findings suggest that a more potent and tissue-selective senolytic, such as the dual BCL-xL and BCL-2 PROTAC 753b, may offer some advantages to inhibit the progression of MASLD and reduce MASH-driven HCC compared to some of the more widely used pan-senolytics. Compared to these senolytics, 753b is less toxic than ABT263 (ref. 28) and more effective than D+Q[54]. Furthermore, its tissue-selective senolytic activity can potentially further reduce some of the health risks associated with systemic clearance of SnCs by the pan-senolytics. It will be of a great interest to determine if additional modification and optimization can further improve the safety and senolytic activity of dual BCL-xL and BCL-2 PROTACs for preclinical and clinic development.

Methods

All procedures involving animals described below were approved by the Institutional Animal Care and Use Committees at the University of Florida (UF), Tulane University (TU) and the University of Texas Health San Antonio (UTHSA).

Chemical compounds

The chemical compounds used in this study are listed in Supplementary Table 2. The synthesis, purification and chemical analysis of 753b were previously published[28].

Cell culture

Human WI-38 fibroblasts (cat. no. CCL-75), HUVECs (cat. no. CRL-1730), RECs (cat. no. PCS-400-012), PACs (cat. no. PCS-210-010), AML-12

cells (cat. no. CRL-2254) and HepG2 cells (cat. no. HB-8065) were purchased from the American Type Culture Collection (ATCC). Huh7 cells (cat. no. 300156) were ordered from Cytion (Cell Lines Service (CLS)). WI-38, HepG2 and Huh7 cells were cultured in complete DMEM (Thermo Fisher Scientific, cat. no. 12430054) supplemented with 10% heat-inactivated FBS (Avantor, cat. no. 1500-500GH), 100 U ml^{-1} penicillin and 100 µg ml^{-1} streptomycin (Thermo Fisher Scientific, cat. no. 15140122) in a humidified incubator at 37 °C and 5% CO_2. HUVECs were cultured in an EGM-2 BulletKit (Lonza, cat. no. CC-3162) containing basal medium and SingleQuots supplements required for growth of HUVECs. RECs were cultured in an REGM-2 BulletKit (Lonza, cat. no. CC-3190) containing basal medium and SingleQuots supplements required for growth of RECs. PACs were cultured in fibroblast basal medium (ATCC, cat. no. PCS-201-030) supplemented with Fibroblast Growth Kit-Low serum (ATCC, cat. no. PCS201041). AML-12 cells were cultured in DMEM/F-12 (Thermo Fisher Scientific, cat. no. 11320033) with the supplementation of 10% FBS, 100 U ml^{-1} penicillin and 100 µg/ml streptomycin, 5 µg ml^{-1} ITS-M (MilliporeSigma, cat. no. I1884-1VL) and 40 ng ml^{-1} dexamethasone (MilliporeSigma, cat. no. D4902-25MG).

Senescence induction

Senescence was induced in WI-38 cells, HUVECs, RECs and PACs using previously validated methods[11,57,58]. Two main methods were used to induce senescence, including IR and replicative exhaustion. Low-passage WI-38 cells (<25 passages), HUVECs (<10 passages), RECs (<10 passages) and PACs (<4 passages) were used as NC cells for the induction of senescence. To induce replicative senescence (REP-SnCs), WI-38 cells, HUVECs and RECs were subcultured until they stopped dividing and became irreversibly cell cycle arrested after 38 passages (WI-38), 22 passages (HUVEC) and 30 passages (REC), respectively. To induce senescence by IR, WI-38 cells, HUVECs, RECs and PACs were subjected to 20-Gy X-ray IR using an X-ray irradiator (Precision, model XRAD-350). IR was used to induce senescence in the mouse hepatic cell line AML-12 using a modified method based on a published protocol[59]. In brief, AML-12 cells that were seeded at approximately 50% confluence in a 100-mm cell culture treated dish were subjected to 20-Gy IR and cultured with basal medium (DMEM-12) containing 5% FBS and 1% penicillin–streptomycin for 2 d. Afterwards, AML-12 cells were subcultured in complete growth medium until they became senescent in about 10 d.

Animal studies

Aged animal study. Male C57BL/6 mice of various age groups (young mice ≤4 months, naturally aged mice ≥20 months) were obtained from the National Institute on Aging. They were maintained in the AAALAC-certified animal facility at UF. Mice were group housed and received food and water ad libitum. The experimental design for evaluating 753b in naturally aged mice is presented in Fig. 2a. In brief, naturally aged mice were randomly assigned to two groups: the vehicle group received IP injections of vehicle composed of 50% PHOSAL 50 PG, 45% MIGLYOL 810 N and 5% Polysorbate 80 (100 µl per mouse, q3d, $n = 6–8$ mice); the 753b treatment group received IP injections of 753b (5 mg kg^{-1}, 100 µl per mouse, q3d, $n = 6–8$ mice) formulated in the vehicle. A group of untreated young mice was included as controls. Seven days after the last injection, mice were euthanized by CO_2 suffocation and cervical dislocation for harvesting various tissues for analysis.

STAM mouse study. The designs of the four STAM mouse studies are presented in Figs. 4a, 6a, 7a and 8a and Extended Data Fig. 5. These studies were done in the AAALAC-certified animal facilities at UF and TU. In brief, the STAM mouse model was generated by subjecting male C57BL/6 mice at P2 to a single subcutaneous injection of 200 µg of STZ. Starting at P30, mice were fed with 60% kcal HFD (Research Diets, D12492) ad libitum to induce MASLD. Mice were randomly assigned to vehicle-treated or 753b-treated groups. For the study shown in Fig. 4, STAM mice were given vehicle or 753b by IP injection (5 mg kg^{-1}, 100 µl per mouse, twice a week, $n = 5$ mice) from P45 to P150. For the early treatment study shown in Fig. 6, STAM mice were given vehicle or 753b by IP injection (5 mg kg^{-1}, 100 µl per mouse, twice a week, $n = 5$ mice) from P45 to P90. For the delayed treatment study shown in Fig. 7, STAM mice were given vehicle or 753b by IP injection (5 mg kg^{-1}, 100 µl per mouse, twice a week, $n = 5$ mice) from P90 to P150. For the late treatment study shown in Fig. 8, STAM mice were given vehicle or 753b by IP injection (5 mg kg^{-1}, 100 µl per mouse, twice a week, $n = 5$ mice) on P145 when the HCC already developed and continued to P175. Vehicle controls for each STAM mouse study were given IP injections of vehicle as described above in a similar manner as 753b-treated mice. Mice were euthanized on P150 for all the studies except the late treatment study, for which mice were euthanized on P175. Tissues were then harvested for analysis.

Study with HCC mouse model induced by HTVi of oncogenes. The design of the study is presented in Fig. 8d. Male FVB/NJ mice were obtained from The Jackson Laboratory at 3–4 weeks of age. They were fed with regular diet throughout the study. After at least 1 week of acclimatization in the UTHSA animal facility, they were hydrodynamically injected via tail vein (HTVi) with an amount of PBS equivalent to 10% of mouse body weight within 7–9 s. The PBS contained plasmids of ΔN90 β-catenin and c-MET at 1 µg g^{-1} body weight and a Sleeping Beauty transposase at 0.08 µg g^{-1} body weight[60]. HCC development was monitored by measuring plasma levels of AFP. After rising AFP levels indicating tumor growth at week 3, mice were randomly assigned into two groups: vehicle group and 753b-treated group. They were subjected to IP injections of vehicle or 753b (5 mg kg^{-1}, twice a week) at week 4. HCC progression in these mice was monitored by analysis of blood levels of AFP. All the mice were euthanized at week 9.5, when both vehicle-treated and 753b-treated mice showed significantly high blood levels of AFP levels and/or external sign of liver tumor growth, by CO_2 inhalation followed by cervical dislocation. Tissues were then harvested for analysis.

Analysis of blood platelet counts. Approximately 50 µl of blood was collected at different timepoints from each mouse via submandibular plexus route in EDTA tubes (RAM Scientific), and platelets were enumerated using an automated hematology analyzer (Drew Scientific, HEMAVET 950FS)[61].

IP ITT. One week before the termination of the experiment on P150, STAM mice were fasted for 3 h and then received IP injection of insulin (0.2 U g^{-1} body weight) (Heartland Veterinary Supply and Pharmacy). Blood glucose levels at 0 min, 30 min, 60 min, 90 min and 120 min after injection were measured in tail vein blood using Precision Xceed with blood glucose test strips (Abbott Japan).

MRI. The MRI study was performed on a 4.7-T/33-cm horizontal bore MR system (Agilent) equipped with a VNMRS Direct Drive console running vnmrj 4.1 at the McKnight Brain Institute at UF. An RRI BFG 200/115-S14 active-shield gradient coil with inner diameter of 115 mm with maximum gradient strength of 670 mT/m at rise-time of 100 µs and a home-bulit 35-mm quadrature transmit/receive volume coil were used for the study. Anesthesia was maintained with 1.5% isoflurane, and body temperature was monitored using a warm air fan (SA Instruments). Data acquisition was synchronized with respiration triggering (SA Instruments).

MRI scans were performed at 3 d before the termination of the experiment on P150. After positioning the mice in the magnet with the heart in the magnet iso-center, reference images of the abdomen using a gradient echo sequence were obtained. Serial of contrast-enhanced

(CE)-MRI measurements of axial and coronal images of mouse liver were performed using a T1-weighted gradient echo sequence with respiratory triggering to cover the whole liver region before and after contrast injection. The parameters used were as follows: repetition time/echo time, 85.5/2.69 mis; NA = 4; flip angle, 20°; field of view, 34 × 34 mm^2; matrix, 128 × 128; number of slices, 16; and slice thickness, 1 mm without gap. Eovist/primovist (Gd-EOB-DTPA) was used to enhance liver tumors. After pre-contract scans, Gd-EOB-DTPA (0.025 mmol Gd/kg body weight) was injected into the tail vein of the mice via a 27-gauge indwelling needle connected to an extension tube and a 1.0-ml syringe. The same scans were repeated at intervals of 45 s for up to 90 min after contract injection.

AFP assay. Blood was collected from the submandibular (facial) vein in heparin tubes. Plasma levels of AFP were measured using Mouse Plasma AFP ELISA kits (cat. no. EK1661) from Boster Bio according to the manufacturer's instructions.

Western blotting

Proteins were extracted from cell samples by lysing cells in 1× RIPA buffer (Boston BioProducts, cat. no. BP-115X) supplemented with 1% protease inhibitor cocktail (Sigma-Aldrich, cat. no. P8340). Protein extraction from mouse liver tissue was performed by using RIPA buffer with protease inhibitor cocktail using a tissue homogenizer. Protein concentration was measured and normalized using the Pierce BCA Protein Assay Kit (Thermo Fisher Scientific, cat. no. 23225). Equal amounts of protein were separated on 4–20% precast polyacrylamide gels (Bio-Rad; Mini-PROTEAN TGX, cat. no. 456-1094) and then transferred to 0.2 µM PVDF membranes. The membranes were then blocked in 1× TBST buffer (Santa Cruz Biotechnology, cat. no. sc-362311) containing 5% non-fat dry milk (Santa Cruz Biotechnology, cat. no. sc-2324) and then probed with primary antibodies overnight at 4 °C. After three washes with 1× TBST, the membranes were incubated with horseradish peroxidase (HRP)-conjugated secondary antibodies for 1–2 h at room temperature. After three washes with TBST, the membranes were incubated in chemiluminescent HRP substrate (MilliporeSigma, cat. no. WBKLS0500) and recorded using a ChemiDoc MP Imaging System (Bio-Rad). All antibodies used in western blot analyses are listed in Supplementary Table 3. ImageJ version 1.52a software (http://rsb.info.nih.gov/ij/) was used for quantification of the immunoblots.

Cell viability assay

For cell viability assays, cells were seeded at previously optimized cell densities in wells of 96-well plates in 100 µl of complete cell growth medium per well. Upon attachment overnight, cells were treated with various compounds (ABT263 and 753b) or vehicle (DMSO). After 72 h of treatment, cell viability was measured using either the tetrazolium-based MTS assay (Promega, cat. no. G1111) or PrestoBlue Cell Viability Reagent (Thermo Fisher Scientific, cat. no. A13262) according to the instructions of the manufacturers. The data were presented as average percentage of cell viability and fitted in nonlinear regression model using GraphPad Prism 9 or 10 software for the generation of dose–response curves and the calculation of half-maximal effective concentration (EC_{50}) values of compounds.

Quantitative RT–PCR

Total RNA was extracted from cells or approximately 25 mg of frozen mouse tissue using RNeasy Mini kits (Qiagen, cat. no. 74106). The downstream procedures for RT–PCR were performed as described previously[11,28]. The list of primers used with the TaqMan Fast Advanced Master Mix (Thermo Fisher Scientific, cat. no. 4444965) is given in Supplementary Table 4. The list of primers used with the Fast SYBR Green Master Mix (Thermo Fisher Scientific, cat. no. 4385617) is given in Supplementary Table 5.

SA-β-gal staining and quantification

SA-β-gal staining in cells was performed using a Senescence β-Galactosidase Staining Kit (Cell Signaling Technology, cat. no. 9860) following the manufacturer's instructions. Cells stained positive by SA-β-gal were counted manually in three fields for each group. Frozen mouse livers in optimal cutting temperature (OCT) compound blocks were sectioned (10 µm thick) and then fixed in 4% formaldehyde for 1 min at room temperature. The sections were then washed in PBS two times for 3 min each time. Sections were then stained in β-gal staining solution (2 mM $MgCl_2$, 150 mM NaCl, 40 mM citric acid, 5 mM potassium ferrocyanide, 5 mM potassium ferricyanide and 1 mg ml^{-1} 5-bromo-4-chloro-3-indolyl/3-D-galactoside (X-Gal) in dimethylformamide stock solution containing 40 mM citric acid and phosphate buffer, pH 6.0) at 37 °C. After the staining, sections were the rinsed twice in PBS and then mounted with aqueous mount solution for observation. Percentage of SA-β-gal-stained areas was quantified using FIJI/ImageJ software according to a previously reported protocol[62].

Cell proliferation assay

EdU staining in cells was performed using a Click-iT EdU Cell Proliferation Kit for Imaging and Alexa Fluor 488 dye (Thermo Fisher Scientific, cat. no. C10337) according to the manufacturer's instructions. Cells stained positive for EdU were counted manually in three fields for each group. Images were taken with Life Technologies EVOS FL Auto Imaging System.

PK and 753b tissue distribution studies

The PK and 753b tissue distribution studies were done by the contract research organization (CRO) Bioduro-Sundia. For the PK study (study no. UFG-FFS-PK-20191113-01), male C57BL/6 mice (7–9 weeks of age) were given 753b (dissoved in 5% DMSO/3% Tween 80 in PBS with 17 meq of 1 N HCl) at 2 mg kg^{-1} or 20 mg kg^{-1} via intravenous or IP injection, respectively. Blood was collected from the mice at various timepoints after a single injection and analyzed for plasma concentrations of 753b using a pre-validated mass spectrometry method. For the tissue distribution study (study no. DIL-FFS-PK-20220113-01V2), male C57BL/6 mice (7–9 weeks of age) were given 753b (5 mg kg^{-1}) via IP injection. They were euthanized at different timepoints after injection to harvest various tissues for analysis. The concentration of 753b in each tissue was measured by using mass spectrometry. For the PK study, samples from three mice at each timepoint were collected and analyzed; for the tissue distribution studies, samples from two mice at each timepoint were collected and analyzed.

Immunofluorescent staining and histological analysis

Liver samples were fixed in 4% buffered paraformaldehyde. Histological analyses were performed with standard protocols using OCT compound or paraffin-embedded sections (6 µm). All antibodies used in immunohistochemistry staining are listed in Supplementary Table 6. Detection was carried out according to the manufacturer's instructions using an ABC Elite kit with ImmPACT DAB substrate (Vector Laboratories). Oil Red O staining was performed as follows. The frozen tissue sections were air dried for 30 min and fixed in 10% formalin for 5 min. The slides were washed with 60% isopropanol and then stained with Oil Red O working solution (Sigma-Aldrich). In addition, Sirius Red staining was performed to detect collagen deposition according to a published method[63]. For estimation of stained positive areas, images were captured with CellSens software using an Olympus BX 51 upright fluorescence microscope outfitted with an Olympus DP80 camera, Plan Fluorite objectives and an LED transmitted light source (Olympus). Stained areas were quantified from 10 random fields of images using ImageJ software and an immunohistochemical profiler according to published methods.

Hydroxyproline assay

Frozen liver samples (20 mg) in 200 µl of water were hydrolyzed in 6 N HCl at 120 °C in a pressure-tight polypropylene vial with PTFE-lined cap for 3 h. After centrifugation at 10,000*g* for 3 min, 50-µl aliquots of supernatant were transferred to wells of a 96-well plate. Sample wells were evaporated to dryness by placing plates in a 60 °C oven. The samples were then incubated with 100 µl of chloramine T/oxidation buffer mixture for 5 min. After adding 100 µl of the diluted 4-(dimethylamino) benzaldehyde reagent to each sample, they were incubated for 90 min at 60 °C before measuring the absorbance at 560 nm. The hydroxyproline content was expressed as µg per g of liver tissue.

Liver function assessment

Liver function tests were carried out in the STAM mice on P150 using the blood samples collected from the mice after they were euthanized. Serum levels of ALT and AST were analyzed using Sigma-Aldrich kits according to the manufacturer's instructions.

Statistics and reproducibility

No statistical methods were used to pre-determine sample sizes, but our sample sizes are similar to those reported in previous publications[11,14]. In animal experimentation, no method of randomization was used, but mice were assigned between experimental and control groups to ensure equivalent baseline for key covariates (such as body weight) between groups. Investigators were not blinded to the conditions of the studies. Naturally aged mice with tumors and/or leukemia were excluded from the experiments if tumors were seen at the autopsy and whole blood cell counts showed abnormalities (25% more or less than normal ranges in white blood cell counts). All data are presented as mean ± s.d. (for data from technical replicates) or mean ± s.e.m. (for data from biological replicates or different mice). Statistical analyses were performed with GraphPad Prism 9 or 10. Comparisons were conducted using unpaired, two-tailed Student's *t*-test when only two experimental groups were involved. For comparisons among more than two groups, one-way ANOVAs with Sidak's multiple comparisons test or Tukey's multiple comparisons test was primarily used. Excepte for Fig. 2b and Extended Data Fig. 1g, Dunnett's post hoc tests were used. Kruskal–Wallis one-way ANOVA with Dunn's multiple comparisons test was used when one-way ANOVA analysis failed the normality test. Two-way ANOVA was used for Extended Data Fig. 4j. In all analyses, *P* values less than 0.05 were considered statistically significant.

Reporting summary

Further information on research design is available in the Nature Portfolio Reporting Summary linked to this article.

Data availability

Source Data and Supplementary Information are provided with this paper. All other data are available from the corresponding authors upon reasonable request.

References

1. Di Micco, R., Krizhanovsky, V., Baker, D. & d'Adda di Fagagna, F. Cellular senescence in ageing: from mechanisms to therapeutic opportunities. *Nat. Rev. Mol. Cell Biol.* **22**, 75–95 (2021).
2. Gorgoulis, V. et al. Cellular senescence: defining a path forward. *Cell* **179**, 813–827 (2019).
3. Pouwels, S. et al. Non-alcoholic fatty liver disease (NAFLD): a review of pathophysiology, clinical management and effects of weight loss. *BMC Endocr. Disord.* **22**, 63 (2022).
4. Riazi, K. et al. The prevalence and incidence of NAFLD worldwide: a systematic review and meta-analysis. *Lancet Gastroenterol. Hepatol.* **7**, 851–861 (2022).
5. Ahmed, A., Wong, R. J. & Harrison, S. A. Nonalcoholic fatty liver disease review: diagnosis, treatment, and outcomes. *Clin. Gastroenterol. Hepatol.* **13**, 2062–2070 (2015).
6. Fraile, J. M., Palliyil, S., Barelle, C., Porter, A. J. & Kovaleva, M. Non-alcoholic steatohepatitis (NASH)—a review of a crowded clinical landscape, driven by a complex disease. *Drug Des. Devel. Ther.* **15**, 3997–4009 (2021).
7. Harrison, S. A. et al. A phase 3, randomized, controlled trial of resmetirom in NASH with liver fibrosis. *N. Engl. J. Med.* **390**, 497–509 (2024).
8. Ogrodnik, M. et al. Cellular senescence drives age-dependent hepatic steatosis. *Nat. Commun.* **8**, 15691 (2017).
9. Meijnikman, A. S. et al. Evaluating causality of cellular senescence in non-alcoholic fatty liver disease. *JHEP Rep.* **3**, 100301 (2021).
10. Papatheodoridi, A. M., Chrysavgis, L., Koutsilieris, M. & Chatzigeorgiou, A. The role of senescence in the development of nonalcoholic fatty liver disease and progression to nonalcoholic steatohepatitis. *Hepatology* **71**, 363–374 (2020).
11. He, Y. et al. Using proteolysis-targeting chimera technology to reduce navitoclax platelet toxicity and improve its senolytic activity. *Nat. Commun.* **11**, 1996 (2020).
12. He, Y., Zheng, G. & Zhou, D. Senolytic drug development. In *Senolytics in Disease, Ageing and Longevity* (eds Muñoz-Espin, D. & Demaria, M.) 3–20 (Springer, 2020).
13. Robbins, P. D. et al. Senolytic drugs: reducing senescent cell viability to extend health span. *Annu. Rev. Pharmacol. Toxicol.* **61**, 779–803 (2021).
14. Chang, J. et al. Clearance of senescent cells by ABT263 rejuvenates aged hematopoietic stem cells in mice. *Nat. Med.* **22**, 78–83 (2016).
15. Jeon, O. H. et al. Local clearance of senescent cells attenuates the development of post-traumatic osteoarthritis and creates a pro-regenerative environment. *Nat. Med.* **23**, 775–781 (2017).
16. Zhu, Y. et al. Identification of a novel senolytic agent, navitoclax, targeting the Bcl-2 family of anti-apoptotic factors. *Aging Cell* **15**, 428–435 (2016).
17. Childs, B. G. et al. Senescent intimal foam cells are deleterious at all stages of atherosclerosis. *Science* **354**, 472–477 (2016).
18. Bussian, T. J. et al. Clearance of senescent glial cells prevents tau-dependent pathology and cognitive decline. *Nature* **562**, 578–582 (2018).
19. Pan, J. et al. Inhibition of Bcl-2/xl with ABT-263 selectively kills senescent type II pneumocytes and reverses persistent pulmonary fibrosis induced by ionizing radiation in mice. *Int. J. Radiat. Oncol. Biol. Phys.* **99**, 353–361 (2017).
20. Yosef, R. et al. Directed elimination of senescent cells by inhibition of BCL-W and BCL-XL. *Nat. Commun.* **7**, 11190 (2016).
21. Ovadya, Y. et al. Impaired immune surveillance accelerates accumulation of senescent cells and aging. *Nat. Commun.* **9**, 5435 (2018).
22. Kolodkin-Gal, D. et al. Senolytic elimination of Cox2-expressing senescent cells inhibits the growth of premalignant pancreatic lesions. *Gut* **71**, 345–355 (2022).
23. Rachmian, N. et al. Identification of senescent, TREM2-expressing microglia in aging and Alzheimer's disease model mouse brain. *Nat. Neurosci.* **27**, 1116–1124 (2024).
24. Ashkenazi, A., Fairbrother, W. J., Leverson, J. D. & Souers, A. J. From basic apoptosis discoveries to advanced selective BCL-2 family inhibitors. *Nat. Rev. Drug Discov.* **16**, 273–284 (2017).
25. Gandhi, L. et al. Phase I study of navitoclax (ABT-263), a novel Bcl-2 family inhibitor, in patients with small-cell lung cancer and other solid tumors. *J. Clin. Oncol.* **29**, 909–916 (2011).
26. Souers, A. J. et al. ABT-199, a potent and selective BCL-2 inhibitor, achieves antitumor activity while sparing platelets. *Nat. Med.* **19**, 202–208 (2013).

27. Leverson, J. D. et al. Exploiting selective BCL-2 family inhibitors to dissect cell survival dependencies and define improved strategies for cancer therapy. *Sci. Transl. Med.* **7**, 279ra40 (2015).
28. Lv, D. et al. Development of a BCL-xL and BCL-2 dual degrader with improved anti-leukemic activity. *Nat. Commun.* **12**, 6896 (2021).
29. Fujii, M. et al. A murine model for non-alcoholic steatohepatitis showing evidence of association between diabetes and hepatocellular carcinoma. *Med. Mol. Morphol.* **46**, 141–152 (2013).
30. Takakura, K. et al. Characterization of non-alcoholic steatohepatitis-derived hepatocellular carcinoma as a human stratification model in mice. *Anticancer Res.* **34**, 4849–4856 (2014).
31. Zhu, Y. et al. The Achilles' heel of senescent cells: from transcriptome to senolytic drugs. *Aging Cell* **14**, 644–658 (2015).
32. Krizhanovsky, V. et al. Senescence of activated stellate cells limits liver fibrosis. *Cell* **134**, 657–667 (2008).
33. Yu, H. et al. Lipid accumulation-induced hepatocyte senescence regulates the activation of hepatic stellate cells through the Nrf2-antioxidant response element pathway. *Exp. Cell. Res.* **405**, 112689 (2021).
34. Saeed, W. K. & Jun, D. W. Necroptosis: an emerging type of cell death in liver diseases. *World J. Gastroenterol.* **20**, 12526–12532 (2014).
35. Krenkel, O. et al. Therapeutic inhibition of inflammatory monocyte recruitment reduces steatohepatitis and liver fibrosis. *Hepatology* **67**, 1270–1283 (2018).
36. Mohammed, S. et al. Necroptosis contributes to chronic inflammation and fibrosis in aging liver. *Aging Cell* **20**, e13512 (2021).
37. Guo, R. et al. Loss of MLKL ameliorates liver fibrosis by inhibiting hepatocyte necroptosis and hepatic stellate cell activation. *Theranostics* **12**, 5220–5236 (2022).
38. Thadathil, N. et al. Senolytic treatment reduces cell senescence and necroptosis in Sod1 knockout mice that is associated with reduced inflammation and hepatocellular carcinoma. *Aging Cell* **21**, e13676 (2022).
39. Slomp, A. & Peperzak, V. Role and regulation of pro-survival BCL-2 proteins in multiple myeloma. *Front. Oncol.* **8**, 533 (2018).
40. Jackson, M. R. et al. Mesothelioma cells depend on the antiapoptotic protein Bcl-xL for survival and are sensitized to ionizing radiation by BH3-mimetics. *Int. J. Radiat. Oncol. Biol. Phys.* **106**, 867–877 (2020).
41. Chen, X. & Calvisi, D. F. Hydrodynamic transfection for generation of novel mouse models for liver cancer research. *Am. J. Pathol.* **184**, 912–923 (2014).
42. He, S. & Sharpless, N. E. Senescence in health and disease. *Cell* **169**, 1000–1011 (2017).
43. Muñoz-Espín, D. & Serrano, M. Cellular senescence: from physiology to pathology. *Nat. Rev. Mol. Cell Biol.* **15**, 482–496 (2014).
44. Muñoz-Espín, D. et al. Programmed cell senescence during mammalian embryonic development. *Cell* **155**, 1104–1118 (2013).
45. Storer, M. et al. Senescence is a developmental mechanism that contributes to embryonic growth and patterning. *Cell* **155**, 1119–1130 (2013).
46. Demaria, M. et al. An essential role for senescent cells in optimal wound healing through secretion of PDGF-AA. *Dev. Cell* **31**, 722–733 (2014).
47. Reyes, N. S. et al. Sentinel *p16*$^{INK4a+}$ cells in the basement membrane form a reparative niche in the lung. *Science* **378**, 192–201 (2022).
48. Helman, A. et al. p16^{Ink4a}-induced senescence of pancreatic beta cells enhances insulin secretion. *Nat. Med.* **22**, 412–420 (2016).
49. Yoshimoto, S. et al. Obesity-induced gut microbial metabolite promotes liver cancer through senescence secretome. *Nature* **499**, 97–101 (2013).
50. Sasaki, M. et al. Bile ductular cells undergoing cellular senescence increase in chronic liver diseases along with fibrous progression. *Am. J. Clin. Pathol.* **133**, 212–223 (2010).
51. Grosse, L. & Bulavin, D. V. LSEC model of aging. *Aging* **12**, 11152–11160 (2020).
52. Yosef, R. et al. p21 maintains senescent cell viability under persistent DNA damage response by restraining JNK and caspase signaling. *EMBO J.* **36**, 2280–2295 (2017).
53. Wan, Y. et al. Endothelial dysfunction in pathological processes of chronic liver disease during aging. *FASEB J.* **36**, e22125 (2022).
54. Raffaele, M. et al. Mild exacerbation of obesity- and age-dependent liver disease progression by senolytic cocktail dasatinib + quercetin. *Cell Commun. Signal.* **19**, 44 (2021).
55. Li, F. et al. FBP1 loss disrupts liver metabolism and promotes tumorigenesis through a hepatic stellate cell senescence secretome. *Nat. Cell Biol.* **22**, 728–739 (2020).
56. Zhang, M. et al. Hepatic stellate cell senescence in liver fibrosis: characteristics, mechanisms and perspectives. *Mech. Ageing Dev.* **199**, 111572 (2021).
57. Li, W., He, Y., Zhang, R., Zheng, G. & Zhou, D. The curcumin analog EF24 is a novel senolytic agent. *Aging* **11**, 771–782 (2019).
58. He, Y. et al. Inhibition of USP7 activity selectively eliminates senescent cells in part via restoration of p53 activity. *Aging Cell* **19**, e13117 (2020).
59. Tripathi, M., Yen, P. M. & Singh, B. K. Protocol to generate senescent cells from the mouse hepatic cell line AML12 to study hepatic aging. *STAR Protoc.* **1**, 100064 (2020).
60. Tao, J. et al. Modeling a human hepatocellular carcinoma subset in mice through coexpression of met and point-mutant β-catenin. *Hepatology* **64**, 1587–1605 (2016).
61. Khan, S. et al. A selective BCL-XL PROTAC degrader achieves safe and potent antitumor activity. *Nat. Med.* **25**, 1938–1947 (2019).
62. Idelfonso-García, O. G. et al. Protocol to detect senescence-associated β-galactosidase and immunoperoxidase activity in fresh-frozen murine tissues. *STAR Protoc.* **5**, 103009 (2024).
63. Quintas Coentro, J. et al. Collagen quantification in tissue specimens. In *Fibrosis: Methods and Protocols* (ed Rittié, L.) 341–350 (Springer, 2017).

Acknowledgements

This work was supported by US National Institutes of Health (NIH) grants R01 AG063801 (G.Z. and D.Z.), R01 CA242003 (G.Z. and D.Z.), K01 AA024174 (L.P.) and R01 AA028035 (L.P.) as well as a Children's Miracle Research Foundation grant awarded to L.P. This research used resources of the Mays Cancer Center Drug Discovery and Structural Biology Shared Resource (NIH P30 CA054174), the Center for Innovative Drug Discovery (CPRIT Core Facility Award RP210208 and NIST Award 60NANB24D117) and the San Antonio Nathan Shock Center (NIH P30 AG013319). We also thank M. Zeeshan for help with senolytic testing in PACs and S. Khan and D. Lyu for their assistance with some of these studies. The experiment involving HTVi of oncogene expression plasmids was assisted by M. McLaughlin and B. Barre.

Author contributions

L.P. and D.Z. made equal contributions to developing concepts and strategies in this study. Methodologies and techniques used in this study were mainly carried out by Y.Y., N.J.-S., Y.H., C.S., T.T., S.B. and L.P. Additional MRI for liver cancer imaging was performed by C.S., H.Z. and L.P. Synthesis and characterization of 753b was done by P.Z. and W.H., under the supervision of G.Z. Characterization of 753b senolytic

activity in vitro and in naturally aged mice was done by Y.Y. and Y.H., under the supervision of D.Z. The STAM mouse model studies were done by N.J.-S., C.S., T.T. and S.B., under the supervision of L.P., and Y.Y. contributed to some of the analyses of hepatic senescence and fibrosis, under the supervision of D.Z. HTVi-induced HCC mouse model study was done by A.S.H., under the supervision of L.-Z.S. Writing of the original draft was performed by Y.Y., Y.H., L.P. and D.Z. X.-M.Y. and R.H. were involved in experimental design and data interpretation. Review and editing of the paper was performed by all authors.

Competing interests

Y.Y., Y.H., P.Z., W.H., G.Z., L.P. and D.Z. are inventors on patents for the use of BCL-xL PROTACs as anti-tumor agents and senolytics. R.H., G.Z. and D.Z. are cofounders of and have equity in Dialectic Therapeutics, which develops BCL-xL/2 PROTACs to treat cancer. The other authors declare no competing interests.

Additional information

Extended data is available for this paper at https://doi.org/10.1038/s43587-025-00811-7.

Supplementary information The online version contains supplementary material available at https://doi.org/10.1038/s43587-025-00811-7.

Correspondence and requests for materials should be addressed to Liya Pi or Daohong Zhou.

Peer review information *Nature Aging* thanks Thomas Bird and the other, anonymous, reviewer(s) for their contribution to the peer review of this work.

https://doi.org/10.1038/s43587-025-00811-7

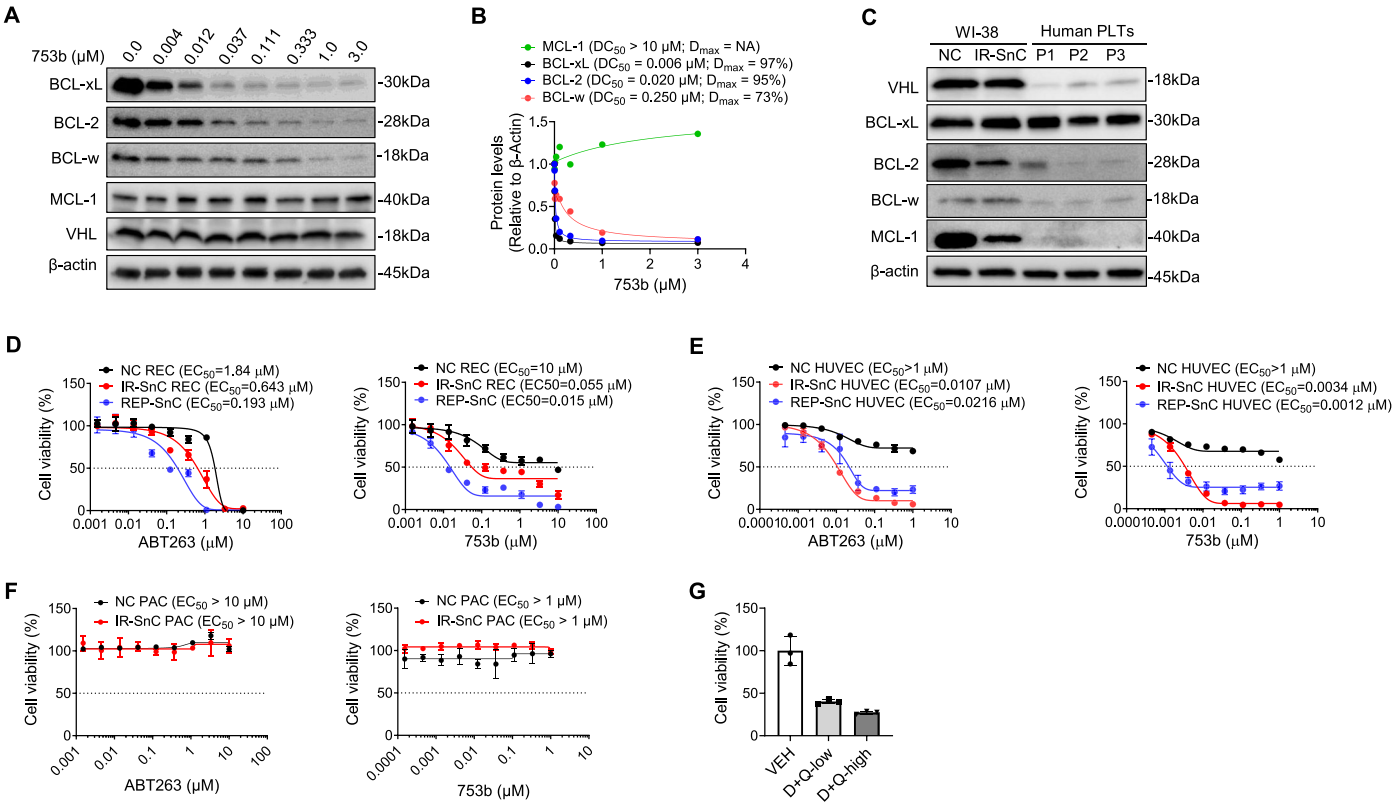

Extended Data Fig. 1 | Evaluation of 753b-induced degradation of the BCL-2 family proteins in WI-38 cells and 753b senolytic activity against renal epithelial cells (RECs), human umbilical vein endothelial cells (HUVECs), and preadipocytes (PACs) *in vitro*. **A**. Representative western blotting images of the levels of BCL-xL, BCL-2, BCL-w, MCL-1, and von Hippel-Lindau (VHL) in NC WI-38 cells after they were treated with increasing concentrations of 753b in a cell culture for 24 h. **B**. Densitometric analyses of BCL-xL, BCL-2, BCL-w, and MCL-1 expression in NC WI-38 cells from **A** are presented. DC_{50}, drug concentration causing 50% degradation of protein of interest; D_{max}, the maximum level of degradation of protein of interest. **C**. The levels of VHL, BCL-xL, BCL-2, BCL-w, and MCL-1 in NC and IR-SnC WI-38 cells and human platelets (PLTs) from three donors (P1-3) were detected by western blotting. Similar results from NC and IR-SnC WI-38 cells were observed in a separate assay. **D-E**. Cell viability analyses show that 753b is more potent than ABT263 against IR-SnC and REP-SnC REC (**D**) and HUVEC (**E**) but less toxic to their non-senescent counterparts. The viability of NC, IR-SnC and REP-SnC REC and HUVEC was determined 72 h after treatment with increasing concentrations of ABT263 and 753b. EC_{50}, half-maximal effective concentration. The data presented are mean ± SD (n = 6 technical replicates) of a representative assay. EC_{50}, half-maximal effective concentration. **F** & **G**. Cell viability analyses show that 753b is not senolytic, but dasatinib and quercetin (D + Q) are, against IR-SnC PAC. The viability of IR-SnC PAC was determined 72 h after treatment with increasing concentrations of ABT263 and 753b (**F**), or with vehicle (VEH), low D + Q (1 μM D plus 20 μM Q) and high D + Q (10 μM D plus 200 μM Q) (**G**). The data presented are mean ± SD (n = 3 technical replicates) of a representative assay. β-actin was used as a loading control in **A** and **C**.

https://doi.org/10.1038/s43587-025-00811-7

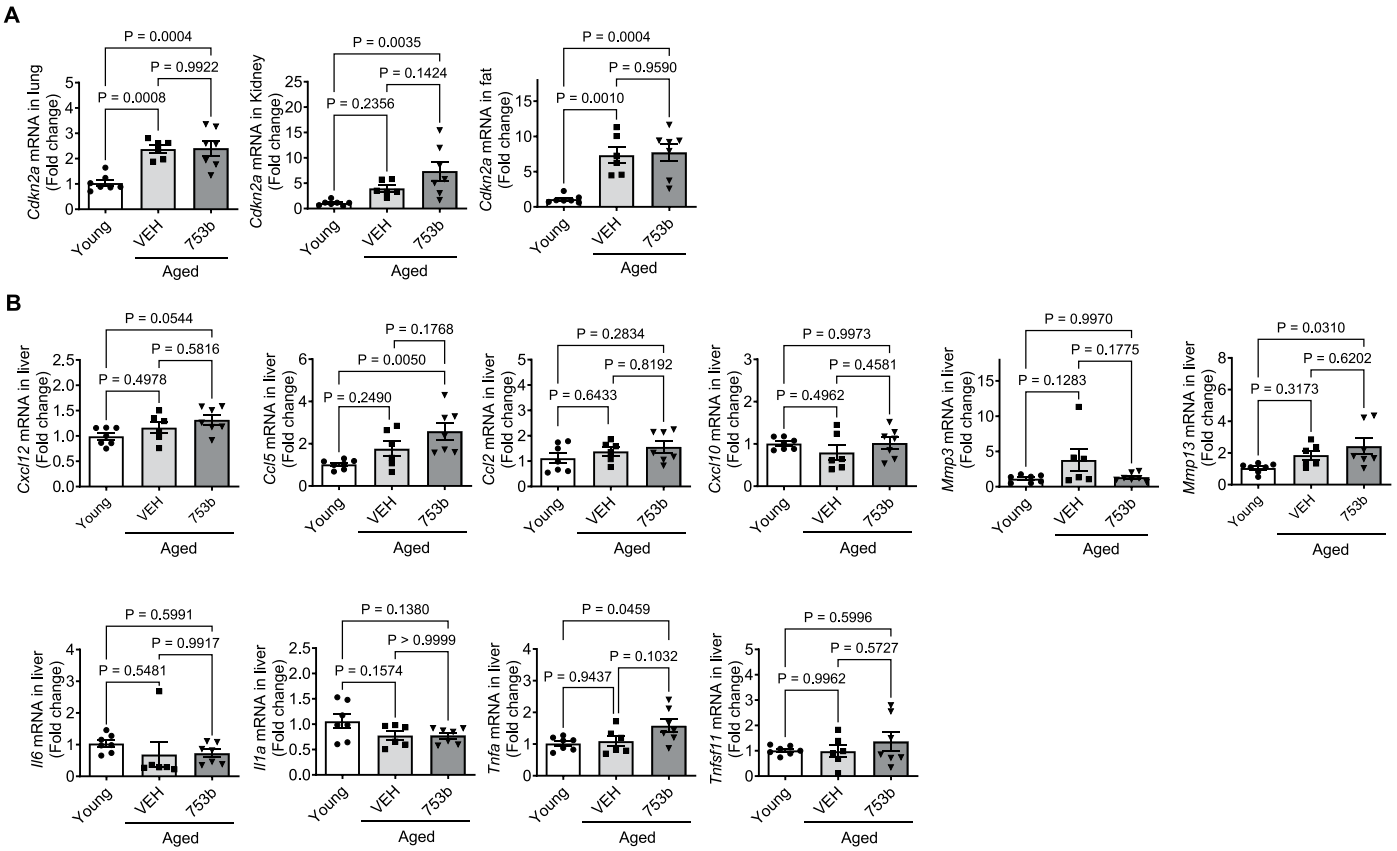

Extended Data Fig. 2 | 753b has no effect on the levels of *Cdkn2a* expression in the lung, kidney and fat tissues but reduces hepatic expression of SASP factors in naturally aged mice. A. The levels of *Cdkn2a* mRNA in the lung, kidney and inguinal fat from untreated young mice and naturally aged mice treated with VEH and 753b. **B**. The levels of *Cxcl12*, *Ccl5*, *Ccl2*, *Cxcl10*, *Mmp3*, *Mmp13*, *Il6*, *Il1a*, *Tnfa*, and *Tnfsf11* in the liver tissue from untreated young mice and naturally aged mice treated with VEH and 753b. The data are presented as means ± SEM (n = 7, 6, and 7 mice per group for young mice, VEH- and 753b-treated aged mice, respectively) and were analyzed by one-way ANOVAs with Šídák's multiple comparisons test or Tukey's multiple comparisons test.

https://doi.org/10.1038/s43587-025-00811-7

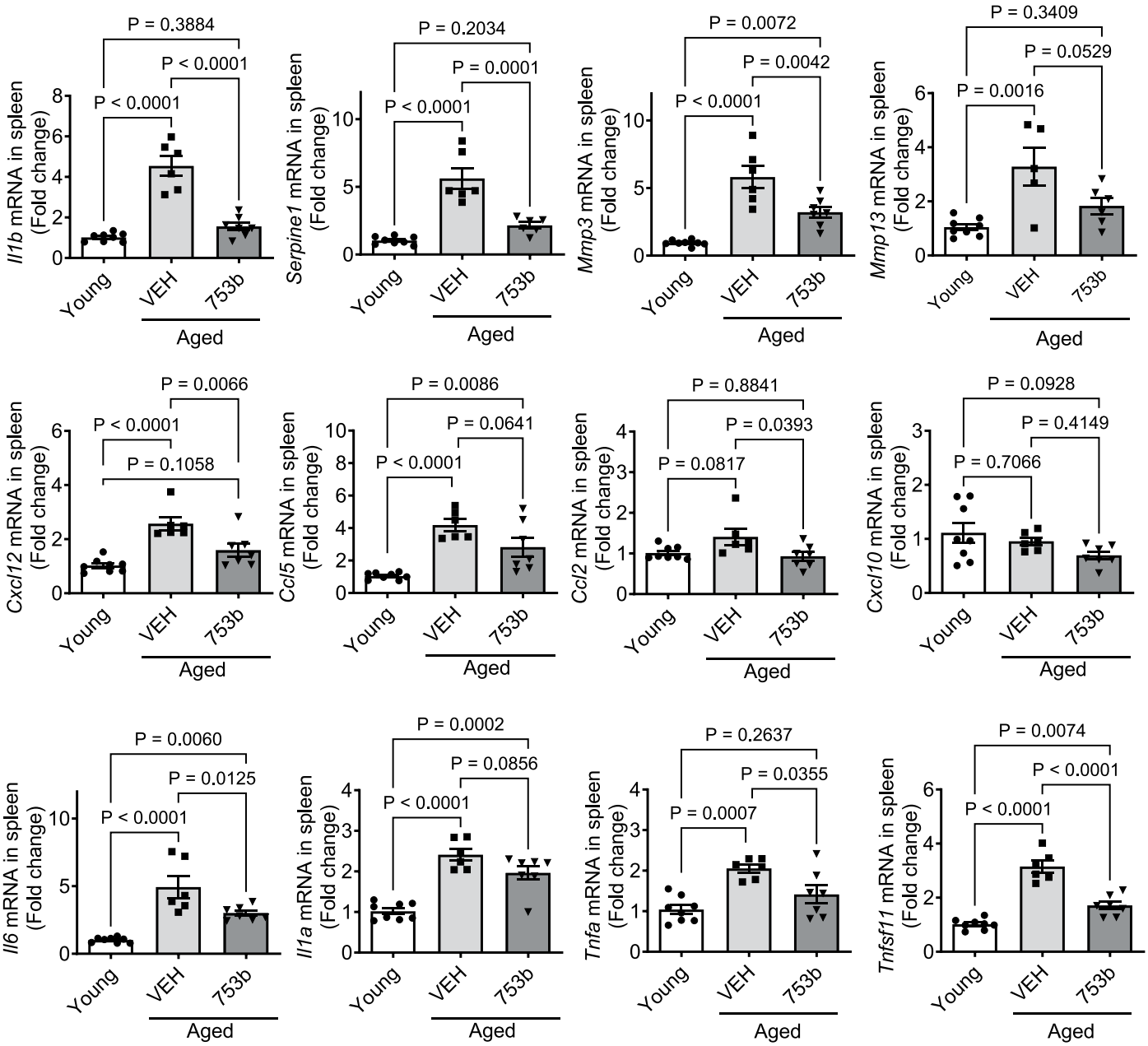

Extended Data Fig. 3 | 753b reduces splenic expression of SASP factors in naturally aged mice. The levels of *Il1b, Serpine1, Mmp3, Mmp13, Cxcl12, Ccl5, Ccl2, Cxcl10, Il6, Il1a, Tnfa*, and *Tnfsf11* in the spleens from untreated young mice and naturally aged mice treated with VEH and 753b. The data are presented as means ± SEM (n = 8, 6, and 7 mice per group for young mice, VEH- and 753b-treated aged mice, respectively) and were analyzed by one-way ANOVAs with Šídák's multiple comparisons test or Tukey's multiple comparisons test.

https://doi.org/10.1038/s43587-025-00811-7

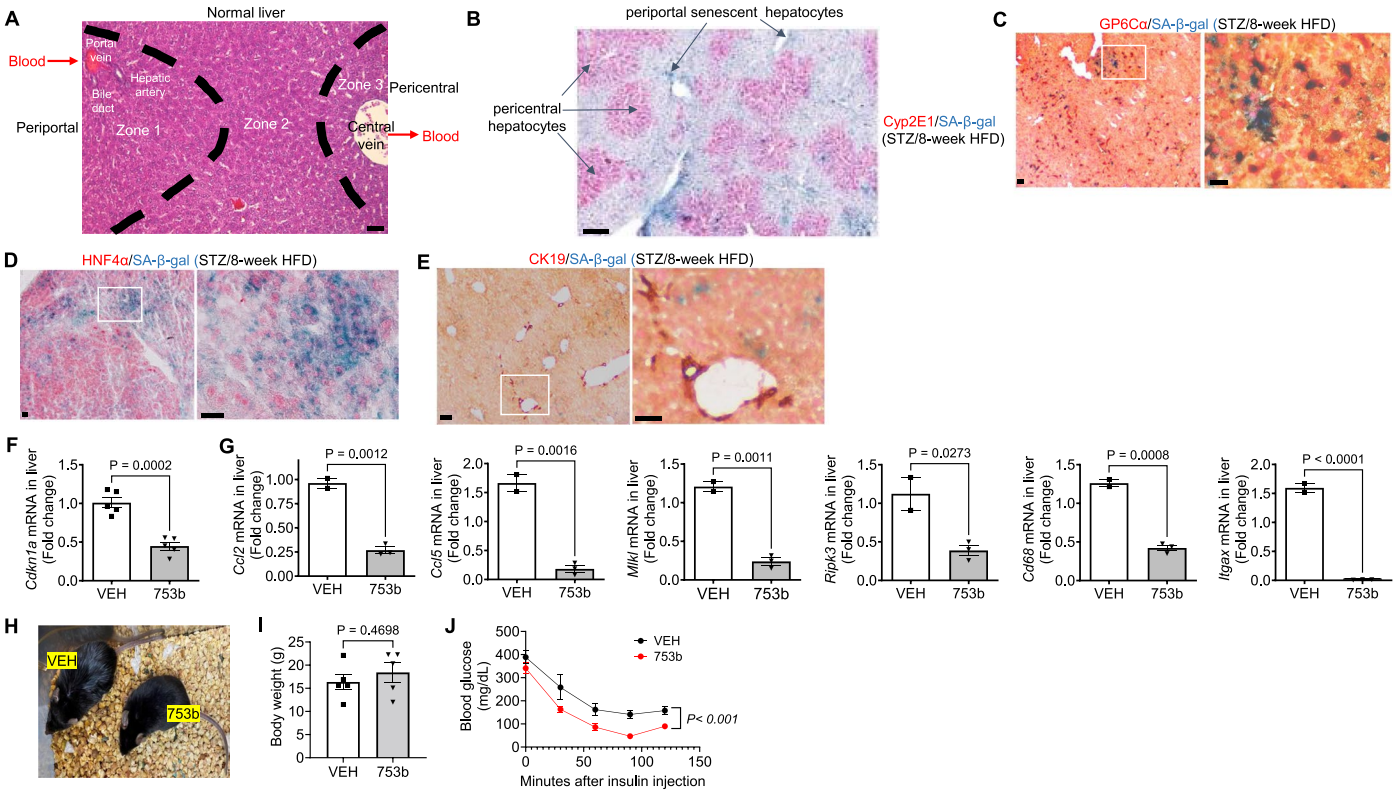

Extended Data Fig. 4 | Characterization of SnCs in the liver from STAM mice and additional evaluations of 753b treatment on STAM mice. A. A cartoon indicates distribution of zone 1, 2, and 3 hepatocytes in liver lobules along with blood flow across the periportal to pericentral axis. Periportal hepatocytes are in zone 1 that consists of portal veins, hepatic arteries, and bile ducts. **B-C**. SA-β-gal staining was combined with immunohistochemistry to characterize types of SnCs in the livers from STAM mice 8 weeks after STZ and 4 weeks after HFD. Antibodies against the pericentral hepatocyte marker Cyp2E1 (**B**), periportal hepatocyte marker GP6Cα (**C**), hepatocyte marker HNF4α (**D**), and biliary epithelial cell marker CK19 (**E**) were used for the stainings. Representative images of the stainings are presented on the left (scale bar = 100 μm) and higher magnification images of the marked area on the left images are presented on the right for **C-E**. Data presented in **A-E** are from one representative experiment and three independent experiments were performed with similar results. **F**. The levels of *Cdkna1* mRNA in the tumor free liver tissues from VEH-treated and 753b-treated STAM mice on P150. The data are presented as means ± SEM (n = 5 mice/group) and were analyzed by a two-tailed, unpaired Student's *t*-test. **G**. The levels of selected SASP mRNA in the tumor free liver tissues from STAM mice on P150. The data are presented as means ± SEM (n = 2 and 3 mice for VEH and 753b group, respectively) and were analyzed by a two-tailed, unpaired *t*-tests. **H**. Photo of reprentative VEH-treated and 753b-treated STAM mice on P150. **I**. Whole body weight of STAM mice on P150. Data are presented as means ± SEM (n = 5 mice per group) and were analyzed by a two-tailed, unpaired Student's *t*-test. **J**. Blood levels of glucose in VEH- and 753b-treated STAM mice after IP injection of insulin one week before the termination of the experiment on P150. Data are presented as means ± SEM (n = 5 mice per group) and analyzed by two-way ANOVA.

https://doi.org/10.1038/s43587-025-00811-7

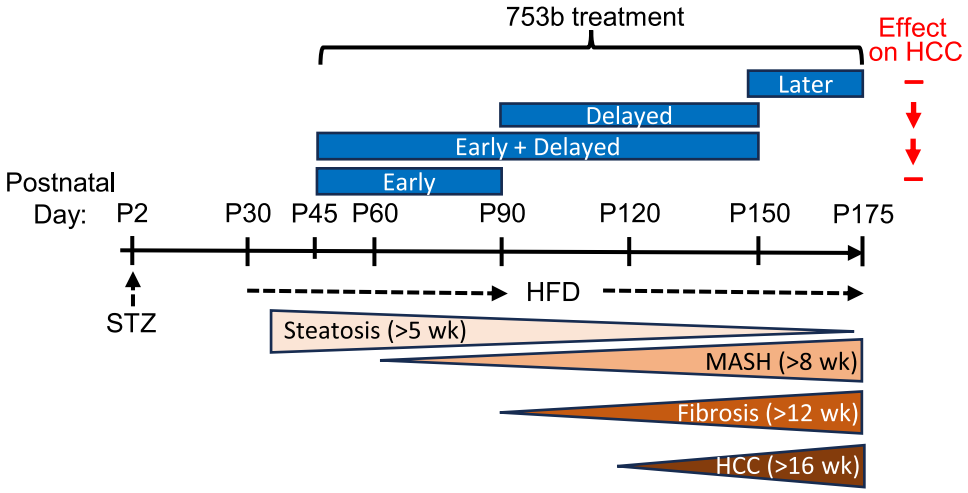

Extended Data Fig. 5 | Diagram illustrating the time-dependent progression of NAFLD and development of HCC in STAM mice and different 753b treatment schedules and their effects on HCC development and progression.

https://doi.org/10.1038/s43587-025-00811-7

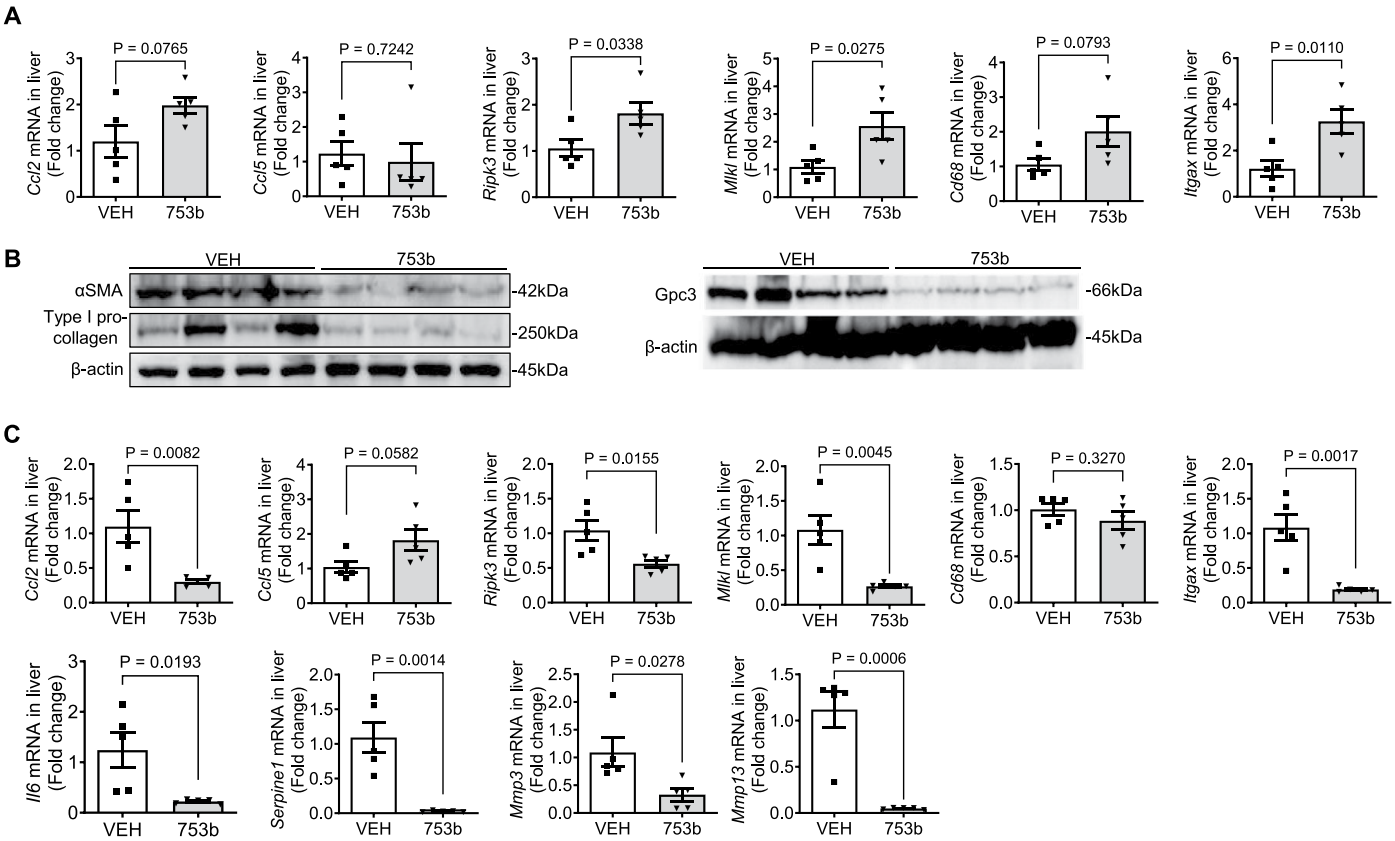

Extended Data Fig. 6 | The effects of early and delayed treatments with 753b on the selective markers of hepatic inflammation, necroptosis, and macrophase activation in the livers from STAM mice. A. The levels of *Ccl2, Ccl5, Mlkl, Ripk3*, and *Itgax/Cd11c* mRNA in the tumor free liver tissues from STAM mice on P150 after receiving earlier VEH or 753b treatment as shown in Fig. 6a. The data are presented in **A** as means ± SEM (n = 5 mice/group) and were analyzed by a two-tailed, unpaired Student's *t*-tests. **B**. Western blotting image of αSMA and Type 1 procollagen in the tumor free liver tissues (left panel), and that of Gpc3 expression in the whole liver tissues (right panel), from STAM mice on P150 after receiving delayed VEH or 753b treatment as shown in Fig. 7a. **C**. The levels of *Ccl2, Ccl5, Il6, Serpine1, Mmp3, Mmp13, Mlkl, Ripk3*, and *Itgax/Cd11c* mRNA in the tumor free liver tissues from STAM mice on P150 after receiving delayed VEH or 753b treatment as shown in Fig. 7a. The data are presented in **C** as means ± SEM (n = 5 mice/group) and were analyzed by a two-tailed, unpaired Student's *t*-tests.

https://doi.org/10.1038/s43587-025-00811-7

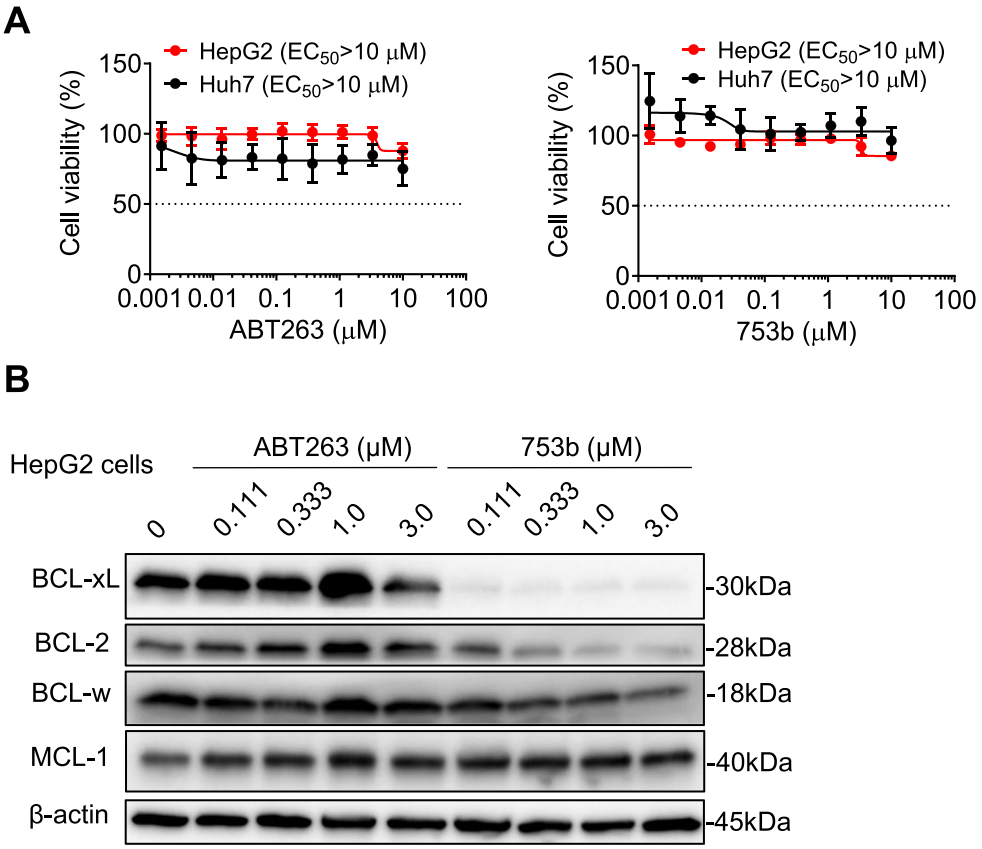

Extended Data Fig. 7 | 753b is not cytotoxic to HCC cells *in vitro*. A. Cell viability of human HCC cells, HepG2 and Huh7, 72 h after treatment with increasing concentrations of ABT263 and 753b in cell culture. EC_{50}, half-maximal effective concentration. The data presented are mean ± SD (n = 6 technical replicates) of a reprentative assay. Similar results were observed in two additional assays. **B.** Representative western blotting images of BCL-xL, BCL-2, BCL-w and MCL-1 in HepG2 cells after they were treated with increasing concentrations of ABT263 and 753b for 16 h. β-actin was used as a loading control.

nature portfolio

Corresponding author(s): Liya Pi, Daohong Zhou

Last updated by author(s): Nov 19, 2024

Reporting Summary

Nature Portfolio wishes to improve the reproducibility of the work that we publish. This form provides structure for consistency and transparency in reporting. For further information on Nature Portfolio policies, see our Editorial Policies and the Editorial Policy Checklist.

Statistics

For all statistical analyses, confirm that the following items are present in the figure legend, table legend, main text, or Methods section.

n/a	Confirmed	
☐	☒	The exact sample size (*n*) for each experimental group/condition, given as a discrete number and unit of measurement
☐	☒	A statement on whether measurements were taken from distinct samples or whether the same sample was measured repeatedly
☐	☒	The statistical test(s) used AND whether they are one- or two-sided *Only common tests should be described solely by name; describe more complex techniques in the Methods section.*
☒	☐	A description of all covariates tested
☐	☒	A description of any assumptions or corrections, such as tests of normality and adjustment for multiple comparisons
☐	☒	A full description of the statistical parameters including central tendency (e.g. means) or other basic estimates (e.g. regression coefficient) AND variation (e.g. standard deviation) or associated estimates of uncertainty (e.g. confidence intervals)
☒	☐	For null hypothesis testing, the test statistic (e.g. *F*, *t*, *r*) with confidence intervals, effect sizes, degrees of freedom and *P* value noted *Give P values as exact values whenever suitable.*
☒	☐	For Bayesian analysis, information on the choice of priors and Markov chain Monte Carlo settings
☒	☐	For hierarchical and complex designs, identification of the appropriate level for tests and full reporting of outcomes
☒	☐	Estimates of effect sizes (e.g. Cohen's *d*, Pearson's *r*), indicating how they were calculated

Our web collection on statistics for biologists contains articles on many of the points above.

Software and code

Policy information about availability of computer code

Data collection	The ChemiDoc MP Imaging System (Bio-Rad, USA) was used to scan all immunoblots. Gen5 version 3.04 software (BioTek, USA) was used for absorbance or luminescence measurements in 96-well plates on Synergy Neo2 multi-mode plate reader. Blood cells (including platelet) were counted using the HEMAVET 950FS hematology analyzer (Drew Scientific, USA). Quantitative PCR were run on an ABI StepOnePlus Real-Time PCR System (Applied Biosystems, USA).
Data analysis	The immunoblots were quantified using the ImageJ version 1.52a software (http://rsb.info.nih.gov/ij/). GraphPad Prism version 9 or version 10 (GraphPad Software, USA) was used for the preparation of all the graphs, determination of half maximal effective concentration (EC50) values, half maximal degradation (DC50) and maximal degradation (Dmax) values, and the statistical analyses.

For manuscripts utilizing custom algorithms or software that are central to the research but not yet described in published literature, software must be made available to editors and reviewers. We strongly encourage code deposition in a community repository (e.g. GitHub). See the Nature Portfolio guidelines for submitting code & software for further information.

Data

Policy information about availability of data

All manuscripts must include a data availability statement. This statement should provide the following information, where applicable:

- Accession codes, unique identifiers, or web links for publicly available datasets
- A description of any restrictions on data availability
- For clinical datasets or third party data, please ensure that the statement adheres to our policy

The source data underlying Fig. 1-8 and Extended Fig.1-7 are provided as separate Source Data files; all unprocessed immunoblots are provided in separate PDF files for Fig. 1, and Fig. 3-5, Extended Fig. 1 and Extended Fig 6-7, unprocessed immunoblots for Supplementary Figure 2 was provided at the end of the Supplementary Information file. All other data are available from the corresponding authors upon reasonable request.

Research involving human participants, their data, or biological material

Policy information about studies with human participants or human data. See also policy information about sex, gender (identity/presentation), and sexual orientation and race, ethnicity and racism.

Reporting on sex and gender	N/A
Reporting on race, ethnicity, or other socially relevant groupings	N/A
Population characteristics	N/A
Recruitment	N/A
Ethics oversight	N/A

Note that full information on the approval of the study protocol must also be provided in the manuscript.

Field-specific reporting

Please select the one below that is the best fit for your research. If you are not sure, read the appropriate sections before making your selection.

☒ Life sciences ☐ Behavioural & social sciences ☐ Ecological, evolutionary & environmental sciences

For a reference copy of the document with all sections, see nature.com/documents/nr-reporting-summary-flat.pdf

Life sciences study design

All studies must disclose on these points even when the disclosure is negative.

Sample size	Sample sizes were designed based on prior experimental experience (Nat Med. 2016 Jan; 22(1): 78-83; Nat Commun. 2020 Apr; 24; 11(1):1996), and similar work on related studies and pilot data.
Data exclusions	Naturally aged mice with tumors and/or leukemia were excluded from the experiments if tumors were seen at the autopsy and whole blood cell counts showed abnormalities (25% > or < than normal ranges in WBC counts). In Extended Fig. 3D, one data point for Serpine1 (753b group) and two data points for Mmp13 (one for VEH group and one for 753b group) was excluded for analysis due to abnormal high values probably resulted from pipetting errors. The data from one VEH group mouse was excluded from analysis due to abnormal low values compared to the rest of the mice in the group, which might be caused by contamination of tumor tissues. We marked the exclusion data in our data Source file.
Replication	To ensure reproducibility of experimental findings, all in vitro assays and some of the in vivo assays were repeated independently at least 2 times except Fig. 2G. One representative result for each experiment is presented in the main Figures or the Extended Data Figures. We confirm that all attempts of replication were successful.
Randomization	Cultured cells were passaged evenly (random distribution) into dishes or flasks for treatment with PROTACs (753b) and/or indicated compounds. In animal experimentation, no method of randomization was used, but mice were assigned between experimental and control groups to ensure equivalent baseline for key covariates (such as body weight) between groups. In cell culture experiments, all wells were inoculated at the same cell density and sequentially assigned to the different treatment groups.
Blinding	Investigators were not blinded during randomizing the aged mice in different groups, because the body weight of the aged mice are not distributed evenly even the mice had the same age. The animals were segregated into separate labeled cages according to the body weight to ensure that each group had animals with similar baseline body weight. For in vitro experiments, investigators were not blinded to the group allocation during the data collection and analysis, because the blinding was not relevant to the study and blinding will negatively affect setting up cell viability assays and Western blotting tests, in these assays treatment group information is needed to make comparison between groups. In STAM mice study, investigators were blinded to allocation during the animal experiments and outcome assessments.

Reporting for specific materials, systems and methods

We require information from authors about some types of materials, experimental systems and methods used in many studies. Here, indicate whether each material, system or method listed is relevant to your study. If you are not sure if a list item applies to your research, read the appropriate section before selecting a response.

Materials & experimental systems

n/a	Involved in the study
☐	☒ Antibodies
☐	☒ Eukaryotic cell lines
☒	☐ Palaeontology and archaeology
☐	☒ Animals and other organisms
☒	☐ Clinical data
☒	☐ Dual use research of concern
☒	☐ Plants

Methods

n/a	Involved in the study
☒	☐ ChIP-seq
☒	☐ Flow cytometry
☒	☐ MRI-based neuroimaging

Antibodies

Antibodies used

Antibodies for Western blot analyses:
Antibody Clone Antibody isotype Catalog # Concentration
Antibody Clone Antibody Isotype Catalog number Concentration
BCL-xL - Rabbit IgG 2764S 1:1000 (Cell Signaling)
BCL-2 D17C4 Rabbit mAb IgG 3498S 1:1000 (Cell Signaling)
BCL-2 EPR17509 Rabbit mAb IgG ab182858 1:500 (Abcam)
MCL1 D2W9E Rabbit IgG 94296 1:1000 (Cell Signaling)
BCL-w 31H4 Rabbit mAb IgG 2724 1:1000 (Cell Signaling)
Caspase 3 - Rabbit IgG 9662 1:1000 (Cell Signaling)
Cleaved caspase 3 Asp175 Rabbit IgG 9661 1:1000 (Cell Signaling)
β-actin 13E5 Rabbit mAb IgG 4970 1:1000 (Cell Signaling)
GAPDH 14C10 Rabbit mAb IgG 2118 1:1000 (Cell Signaling)
VHL - Mouse mAb IgG sc-135657 1:1000 (Santa Cruz)
Gpc3 9C2 Mouse mAb IgG MA5-17083 1:1000 (Proteintech)
αSMA - Rabbit IgG 14395-1-AP 1:1000 (Proteintech)
α-tubulin - Rabbit IgG 11224-1-AP 1:10000 (Proteintech)
Pro-collagen-type I - Rabbit IgG 14695-1-AP 1:1000 (Proteintech)
β-actin 4H1 Rabbit IgG 81115-1-RR 1:10000 (Proteintech)
Secondary antibody - Anti-rabbit IgG 7074S 1:5000 (Cell Signaling)
Secondary antibody - Anti-mouse IgG 7076S 1:5000 (Cell Signaling)
HNF4α H-171 Rabbit sc-8987 1:100 (Santa Cruz)
GP6Cα - Rabbit 22169-1-AP 1:100 (Proteintech)
Cyp2E1 - Rabbit 19937-1-AP 1:200 (Proteintech)
CK19 - Rabbit 10712-1-AP 1:200 (Abcam)

Validation

All the used antibodies are commercially available. The antibodies used in a specific species or application have been validated by manufacturers to be used in that species/application and this information is provided in their website and/or antibody datasheets. Only validated commercial antibodies or antibodies validated in our previous studies were used for immunostaining and Western blotting of cell and mice samples.

Eukaryotic cell lines

Policy information about cell lines and Sex and Gender in Research

Cell line source(s)

Human WI-38 fibroblasts (Cat. No. CCL-75), human HUVEC (Cat. No. CRL-1730), human RECs (Cat. No. PCS-400-012) and human PACs (Cat. No. PCS-210-010) were purchased from the American Type Culture Collection (ATCC, Manassas, VA, USA). AML12, Huh7 and HepG2 cells were kindly provided by Dr. Liya Pi. AML12 and HepG2 cells were originally ordered from ATCC, their respective catalog numbers are CRL-2254 and HB-8065. Huh7 cells were ordered from Cytion (Cat. No. 300156).

Authentication

The cell lines have been validated by the suppliers. All the cell lines used except Huh7 were purchased from ATCC as 'Certified Reference Material' stocks. ATCC authenticates cell lines using morphology, karyotyping and STR profiling. Hub7 cells were obtained from Cytion, which authenticates cell lines using Short Tandem Repeat (STR) profiling.

Mycoplasma contamination

Cell lines were recently purchased from ATCC and were not further tested for mycoplasma contamination in our laboratory, but cell proliferation rate and morphology of all the cell lines were continuously monitored.

Commonly misidentified lines
(See ICLAC register)

none

Animals and other research organisms

Policy information about studies involving animals; ARRIVE guidelines recommended for reporting animal research, and Sex and Gender in Research

Laboratory animals	Female and male 5-6 weeks old and naturally aged C57BL/6 mice were obtained from National Institute of Aging (NIA) and used for the in vivo platelet toxicity assay and evaluation of 753b treatment. All mice were housed in the Assessment and Accreditation of Laboratory Animal Care (AAALAC)-accredited animal facilities at University of Florida (UF) under pathogen-free conditions. Mice with tumors and/or leukemia were excluded from experiments and analyses. 20 months or older male and female mice were considered as naturally aged mice and were randomly assigned to one of the treatment groups (VEH group has all male mice, 753b treated-group has 6 male and 1 female mouse). Mice with tumors and/or leukemia were excluded from experiments and analyses. C57B/L6 breeder (8 week old) were obtained from Jackson laboratory (Bar Harbor, ME), and the offspring were used for developing STAM mice. 3-4 weeks of age Male FVB/NJ mice were purchased from the Jackson Laboratory for HTVi- oncogenes-induced HCC study. All mice were housed in rooms with the standard/default diurnal light cycle: 12-hr light: 12-hr dark (12L: 12D) with the lights being ON during the daytime and OFF during the night time. Mice room conditions were maintained by standards: temperatures of 65-75°F (~18-23°C) with 40-60% humidity.
Wild animals	This study did not involve wild animals.
Reporting on sex	Sex was considered in the in vivo evaluation of 753b treatment. The findings of 753b as an effective senolytic apply to both naturally aged female and male C57B/L6 mice. Evaluation of 753b treatment in the STAM mice model primarily used male mice as it was published that male mice have higher incidence of having non-alcoholic fatty liver disease.
Field-collected samples	This study did not involve filed-collected samples.
Ethics oversight	All animals work was approved and done in accordance with the AAALAC-certified animal facility at University of Florida, except the pharmacokinetic studies that were done by BioDuro (San Diego, CA), a contracted research organization. All animal studies were compiled with the ethical regulations and humane endpoint according to the NIH Guidelines for the Care and Use of Laboratory Animals.

Note that full information on the approval of the study protocol must also be provided in the manuscript.

Plants

Seed stocks	N/A
Novel plant genotypes	N/A
Authentication	N/A